國立交通大學

光電工程研究所

碩 士 論 文

使用共軛焦偏振螢光顯微鏡重建液晶透鏡 3D 內部結構

3D Imaging and Analysis for LC Lens Applications by Fluorescence Confocal Polarizing Microscopy

研 究 生：謝博元

指導教授：謝漢萍　博士

黃乙白　博士

中 華 民 國 一 百 年 六 月

使用共軛焦偏振螢光顯微鏡重建液晶透鏡 3D 內部結構

3D Imaging and Analysis for LC Lens Applications by Fluorescence Confocal Polarizing Microscopy

研 究 生：謝博元　　Student：Po-Yuan Hsieh

指導教授：謝漢萍　　Advisor：Han-Ping D. Shieh

黃乙白　　Yi-Pai Huang

國 立 交 通 大 學

光電工程研究所

碩 士 論 文

A Thesis

Submitted to Institute of Electro-Optical Engineering

College of Electrical and Computer Engineering

National Chiao Tung University

in partial Fulfillment of the Requirements

for the Degree of

Master

in

Electro-Optical Engineering

June 2011

Hsinchu, Taiwan, Republic of China

中華民國一百年六月

使用共軛焦偏振螢光顯微鏡重建液晶透鏡 3D 內部結構

碩士研究生：謝博元　　指導教授：謝漢萍教授

黃乙白副教授

國立交通大學　　光電工程研究所

摘要

在傳統變焦鏡頭中，需要較大空間來配置各個透鏡之間的相對位置。液晶透鏡具有較薄、較輕、可變換焦距等優勢，因此非常適合於手機相機等應用。傳統上，我們藉由量測線性偏振光，經過液晶透鏡後的相位變化條紋(fringing patterns)得以觀察液晶透鏡的各項光學特性。然而相位變化條紋乃是偏振光穿過液晶層的積分結果，無法顯示液晶層內部的資訊細節，如：液晶分子等效折射率、液晶分子排列狀況等。在本篇論文中，我們提出利用共軛焦偏振螢光顯微鏡(Fluorescence Confocal Polarizing Microscopy)重建液晶透鏡內部液晶分子 3D 結構。首先，將螢光分子摻雜於液晶中，藉由量測螢光強度推算液晶分子的轉動角度。更進一步，我們可以繪製出液晶透鏡內部的折射率變化狀況，並重建液晶透鏡的 3D 結構模型，藉此詳細分析光線在液晶層內部的光追跡過程，以及液晶透鏡的光場調變能力。在本篇論文中，我們分析液晶透鏡的折射率分佈，並且推算光波前經過液晶透鏡後的相位延遲變化，藉此推算液晶透鏡的一階光學性質。除此之外，利用共軛焦偏振螢光顯微鏡，我們可以藉由光波前的相位延遲變化，分析傳統相位變化條紋所不能分辨的正、負液晶透鏡特性。

3D Imaging and Analysis for LC Lens Applications by Fluorescence Confocal Polarizing Microscopy

Student: Po-Yuan Hsieh **Advisor: Dr. Han-Ping D. Shieh**

Dr. Yi-Pai Haung

Institute of Electro-Optical Engineering,

National Chiao Tung University

Abstract

Liquid Crystal lenses (LC lenses) are prospective devises in the mobile application, because they are slight and tunable-focus. Conventionally, the fringing patterns are utilized to analyze the optical properties of LC lenses by plotting the bright-dark stripes. However, the fringing pattern must lose some detail information in the LC cells, such as the refractive index distribution and the LC directors.

The Fluorescence Confocal Polarizing Microscopy (FCPM) method for was proposed to image and analyze 3-Dimentional (3-D) directors of LC molecules. By detecting the excited fluorescence of the anisotropic dyes which is doping in the LC cell and can be along the director of LC molecules, the spatial refractive index of deformed LC layer can be calculated. In this thesis, we investigated the spatial variation of LC molecules in the LC lenses. The results of spatial phase retardation were compared by using FCPM method and conventional fringing pattern. The difference of LC lens driven in convex and concave modes was also illustrated by the FCPM method.

誌謝

倏忽，五年的時光就這樣過去了。當初莫名其妙的填上交大光電系，大學部四年，加上碩士班一年，期間經歷了很多事情，遇見了許多人們，都彷彿好像是昨天發生的一樣。首先要感謝的是謝漢萍老師和黃乙白老師的指導，老師們對於英文報告的要求和鼓勵，促使我有極大的成長。特別是黃老師總是勉勵我們要對自己做的東西有信心，在各方面都不斷地給予我們肯定，謝謝您。

其次，我想要感謝液晶組的成員們，凌嶢、玉米、小發特、致維哥、以及該逼，在這倉促的一年間，有太多太多地方都感謝你們無私的幫助。特別是小發特學長，一起做實驗，一起泡在無塵室的日子其實都充滿了淚水和歡笑，除了革命情感之外，再也想不出其他的詞彙。當然還有實驗室裡的同學們，一想到接下來大家就要各分東西，就不禁感傷起來。但是即使分開了，我們也還是夥伴吧!!!

此外，還要感謝光電系的學長學姊學弟學妹們。特別是光電系棒的成員們，雖然被你們酸得很慘，但是一起練球的日子，依然會是我最珍貴的回憶。而信文、菜花、有毅、小樹以及諸位族繁不及備載的國中高中同學們，雖然大家生活都很忙碌，但是每次聚會卻都還是排除萬難的出席，謝謝你們的情義相挺。

最感謝的是我親愛的家人們，感謝你們如此包容一個出門像丟掉，回家像撿到一樣的孩子。無論我想要做什麼事情，你們總是毫無保留的支持我，鼓勵我，安慰我，甚至是在我做錯事的時候大聲斥責我，謝謝你們。還有阿姐，感謝你 24 小時不打烊的人生諮詢服務，還請我看了很多場電影。因此，我很盡責的將你寫在誌謝中，希望明年你也能夠把我放進你的論文誌謝裡面。

僅以這篇論文獻給曾出現在我生命中的所有人。

Contents

Figure Captions

List of Tables

Chapter 1

Introduction

1.1 Tunable-Focus Lenses

Lenses are key elements of optical systems. Most conventional lenses are made of glass, polymer, or other transparent solid materials, which exhibit particular fixed focal lengths. For a tunable-focus imaging systems, it needs a mechanical assembly of conventional lens elements to vary the effective focal length [1]. Zoom lenses, for example, are achieved by adjusting the distance of two or more lenses to vary the effective focal length and simultaneously compensate the deviation of imaging plane to the position of image sensor, as shown in Fig. 1-1 [2]. Therefore, it usually takes large volume for the mechanical movement.

Numbers of conventional lens components also make the zoom lenses system bulky and heavy. In many consumer products, slim and slight would be the key concern, especially in mobile devices. They would benefit from a simpler, slighter, and tunable-focus lens.

In fact, simple tunable-focus lenses have already existed in nature. Human eye, for example, is a singlet lens system with a tremendously wide tunable focus range. With shape change of the crystalline lens in the eye, the effective focal length of the eye could be conformed to the retina, as shown in Fig. 1-2. To mimic the function of human eyes, many similar technologies have been proposed to change the lens shape, including liquid lenses [3-7], and microfluidic lenses [8, 9]. Those tunable-focus lenses usually generate the optical path difference between the center and the edge of the lenses by adjusting the lens thickness. The thinner part of the lens will induce less

phase retardation, and the thicker parts will induce more phase retardation.

General liquid lenses are constructed by the interface between two different materials [10-14]. With electrically or mechanically control on the shape of interfaces, we can appropriately manipulate the lens power, as shown in Fig. 1-3 and Fig. 1-4. The major issues of these technologies are the environmental limitations, such as gravity or low feasible range of temperature.

Liquid Crystal (LC) is also a common material for singlet tunable-focus lens. Instead of the shape changing, LC lenses adjust the refractive index changing to generate the same optical path difference as conventional lenses. LC has been wildly utilized as spatial light modulators in Liquid Crystal Displays (LCDs), because refractive index is sensitive to electrical control [15-18], which means the lens power will be easily controlled by applying voltages. Furthermore, the stability of LCs also favors the industrial fabrications. Therefore, LCs is a unique and suitable material for singlet tunable-focus lenses.

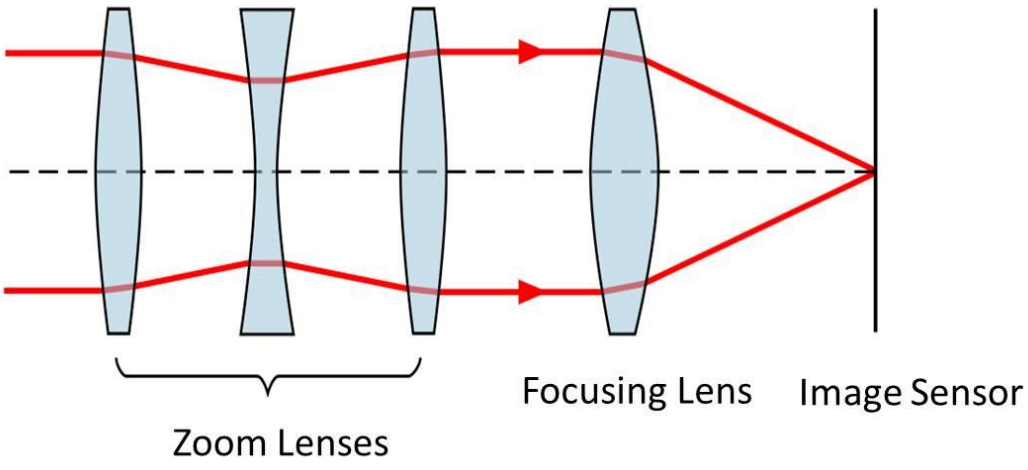

Fig. 1-1 Schematic of simple zoom lens system

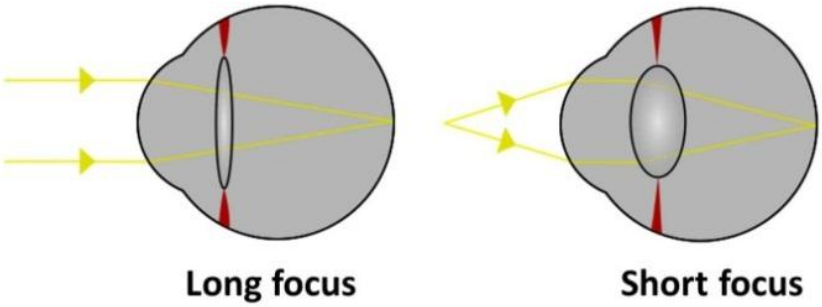

Fig. 1-2 Schematic of the focusing mechanism of human eyes.

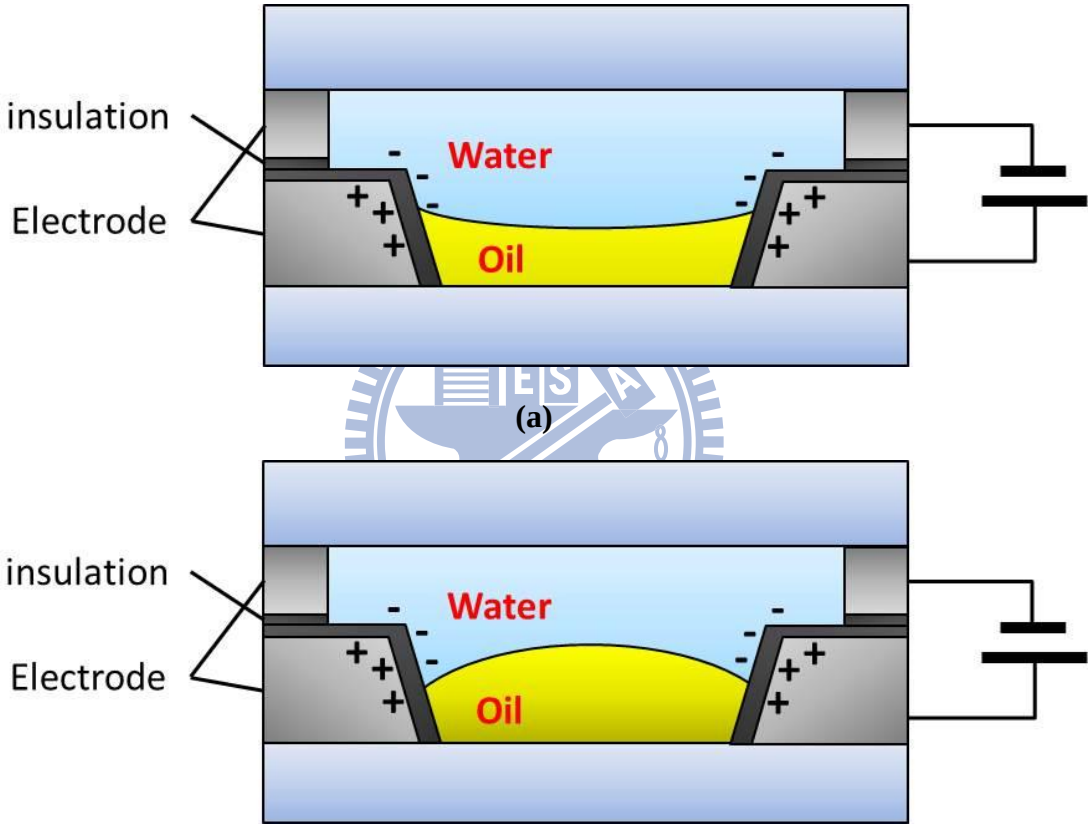

Fig. 1-3 The liquid lens employs the oil-water surface and electrically control the surface shape in (a) concave lens and (b) convex lens mode.

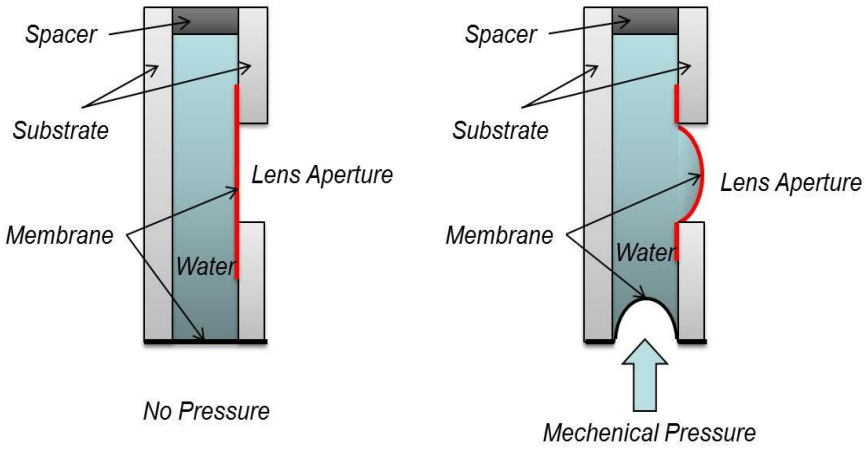

Fig. 1-4 Liquid lens mechanically controlled the membrane shape to focus lights.

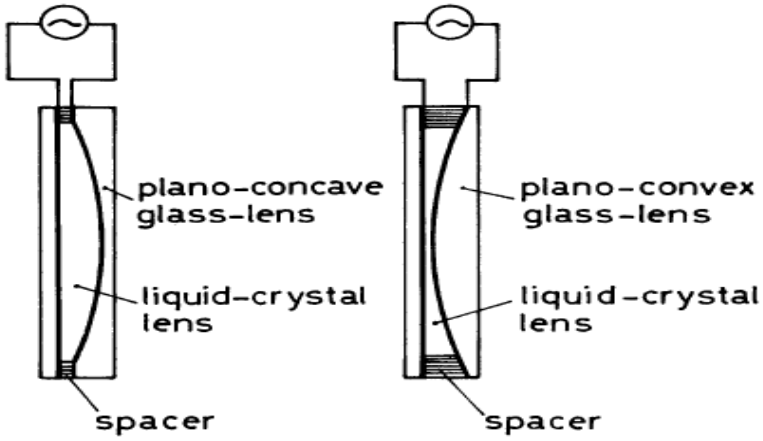

Fig. 1-5 The world first LC lens proposed by Prof. Susumu Sato.

1.2 LC Lenses

Liquid Crystal (LC) was firstly employed for lens application by Prof. Susumu Sato in 1979 [19]. Two plano-concave and plano-convex glass lenses covered by the transparent substrate were prepared, and liquid crystal was injected into the cavity, as shown in Fig. 1-5. During the electrical operation, the LC lens power could be changed without any shape change. The operating voltage would modulate the orientation of LC molecules to control the effective refractive index of the LC lens-cell. The process is tantamount to changing the material of the lens in front of the glass lens. In this LC lens system, the polarizers in front of the LC lens-cells are necessary to yield extraordinary light.

1.2.1 Typical Structures of Liquid Crystal Lenses

Prof. Shin-Tson Wu further classified LC lens structures into three fundamental approaches as following [1, 20-22]:

1. An inhomogeneous electric field applied to a homogeneous LC layer.
2. An inhomogeneous electric field applied to an inhomogeneous LC layer.
3. A homogeneous electric field applied to an inhomogeneous LC layer.

One of the typical structures which controlled by an inhomogeneous electric field applied to a homogeneous LC layer is shown in Fig. 1-6. The indium-tin-oxide (ITO) electrode was deposited on a plane and a concave glass substrate. LC was injected into the cavity between those two ITO-glass substrates. In the voltage-off state, the effective refractive index of LC material is n_e, which is much larger than n_g the refractive index of glass substrates. The LC lens is driven as a convex lens with shorter focal length. While the voltage applying, the effective refractive index of LC material became n_o, which is closer to n_g, thus increases the focal length.

On the other hand, there are also combined structures which including the homogeneous LC layer and inhomogeneous substrate to yield a non-uniform electrical field [23]. The homogeneous LC layer is sandwiched between a flat substrate, and a plano-convex top substrate, as shown in Fig. 1-7. To form the inhomogeneous electric field, ITO electrodes are coated on the convex surface of the top substrate, and the flat surface of the bottom substrate. The curved electrode structure will induce an inhomogeneous electric field which generating a gradient orientation of LC as a lens. The driving voltage can modulate the lens power of the LC layer.

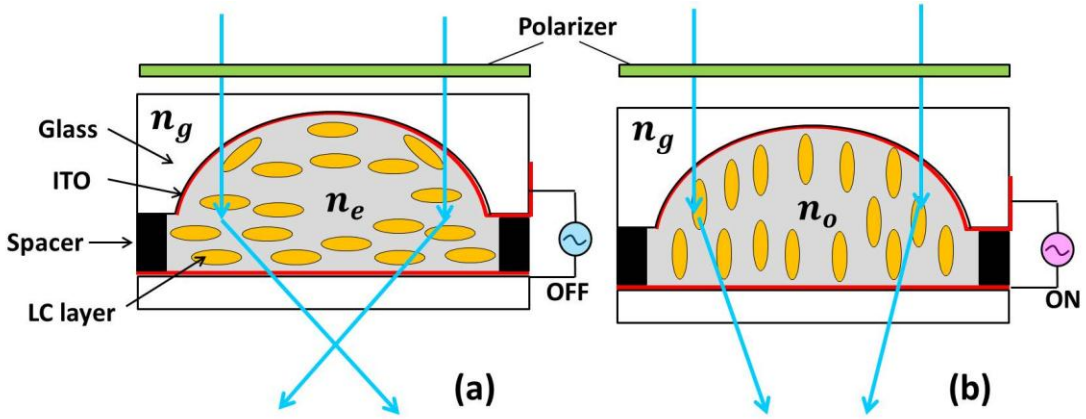

Fig. 1-6 The typical structures controlled by inhomogeneous field with an inhomogeneous layer on (a) short focusing state, and (b) long focusing state.

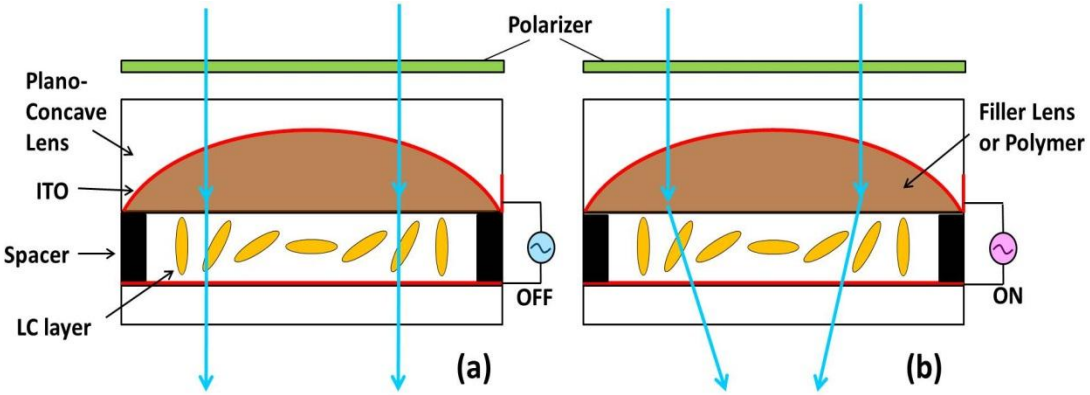

Fig. 1-7 The typical structures controlled by inhomogeneous field with an homogeneous LC layer on (a) un-focusing state and (b) focusing state.

1.2.2 Patterned Electrode of LC Lens

The above approaches of LC lenses all have the same issue that ITO electrode of top substrate needs special manufacture process, which adds the difficulties and costs. A simpler structure of LC lens is achieved by utilizing the fringe field to control the orientation of a homogeneous LC layer. This structure is typically constructed with two flat ITO-glass substrates chipping a homogenous LC layer. The ITO electrodes could be patterned to yield the fringe field which modulating the gradient orientation of LC, as shown in Fig. 1-8.

This kind of structure has advantages of simpler fabricating process and smooth controlling on the focal length. It is also easy to realize the spherical or lenticular lens array applications, depending on different electrode configurations. Therefore, our studies would focus on the patterned electrode LC lenses.

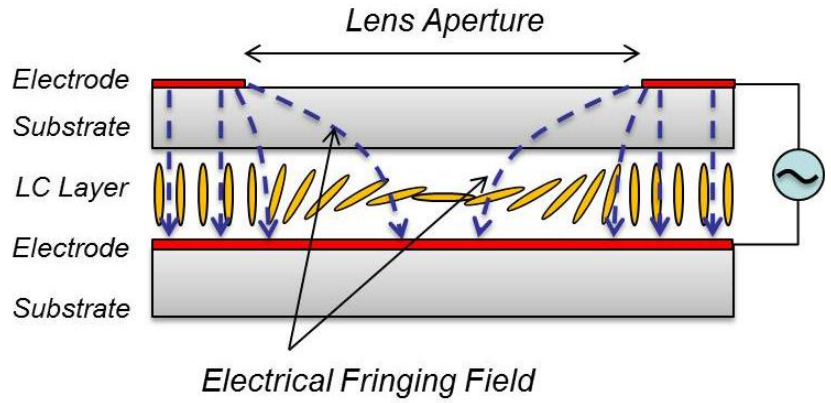

(a)

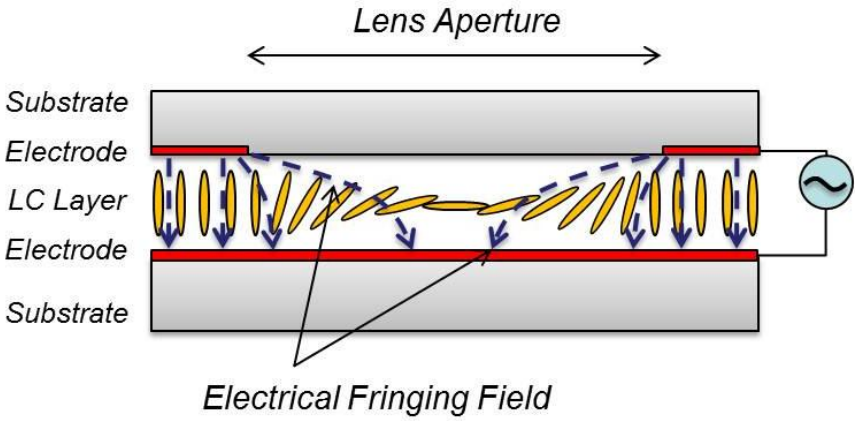

(b)

Fig. 1-8 Two of the most general homogeneous LC Lenses, (a) the structure with external electrodes, and (b) the structure with internal electrodes utilizing electrical fringe field of the electrodes to generate a gradient variation in phase retardation.

1.2.3 Orientation of Liquid Crystals

The lens effects of the typical structure LC lens which with inhomogeneous electric field applied on a homogeneous LC layer are achieved by the gradient orientation of LCs in the lens cell.

In convergent LC lens modes, for example, the LC molecules at the center of the LC lens are steadied with small tilt angles, while large tilt angles are showing on the

edge. As the gradient LC tilt angles distribution which is larger on the edge, the optical path length (OPL) on the edge of the LC lens is smaller oppositely.

As the result of the gradually varied OPL, the phase retardation of incident light on the edge is faster than the center of the LC lens driven as convergent LC lens mode. Simultaneously, the wave front through the convergent mode LC lens will be bended toward the optic axis of the LC lens. In other words, the LC molecules with gradient orientation of lager tilt angle on the edge will effect as the conventional convex glass lenses, as shown in Fig. 1-9.

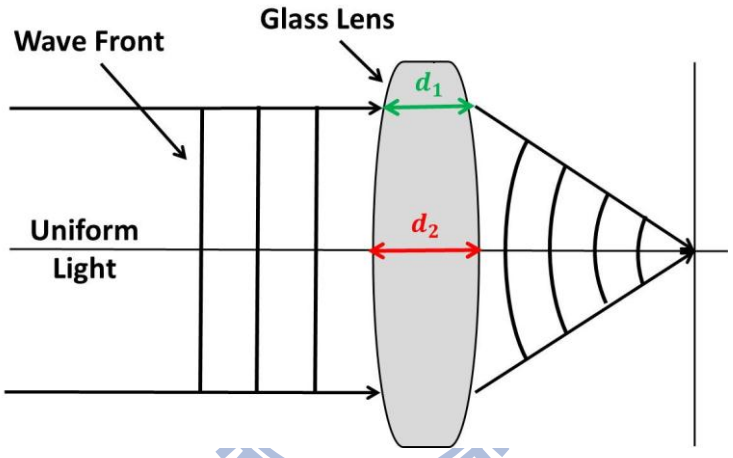

(a)

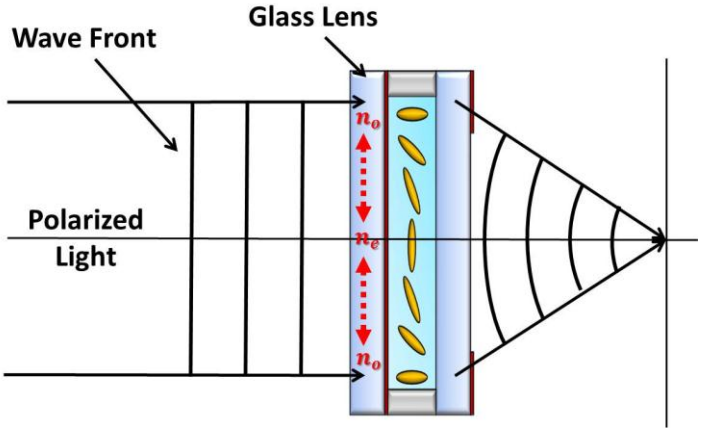

(b)

Fig. 1-9 The wave front will be bended toward the optical axis while propagating through (a) the glass lens, and (b) the LC lens because the optical path difference between at the edge and on the center.

1.3 Motivation and Objective

To investigate the lens performance and other optical properties, the profile of the molecules is usually observed to determine the optical path length (OPL) of the LC lens. Conventionally, the fringing pattern is used for the observation of the relative phase retardation [24]. It employs two crossed polarizers placed in back and front of the LC lens to measure the intensity of the incident light passing the lens. As the polarized light from the first polarizer is modulated by the lens, the polarizations are changed and analyzed by the second polarizer. It is convenient to capture the fringing pattern of the final output light for measuring the phase retardation. By plotting the profile of the white-black pattern, called fringing pattern, the variation of the OPL can be calculated to estimate the optical properties.

However, the fringing pattern is an absolute integral result of light wave front traveling through whole LC lens, which is difficult to observe the significant behavior of light in the LC cells. This may lose the detail information which is important for LC lens analysis, such as the spatial director of LC molecules, the distribution of refractive index, and the propagation of light in LC lenses, as shown in Table 1-1. For example, the fringing patterns of a cylindrical LC lens with tree parallel electrodes driven in convex and concave modes are similar, as shown in Fig. 1-10, but the optical properties are totally different. The modes can only identify by the driving voltages of each electrode or the focusing result. Therefore, fringing pattern only shows the relative phase losing the certain values. Furthermore, if there is defect or other significant behavior of LC molecule, this approach is difficult for analysis.

To significantly construct the 3-dimensional (3-D) image of LC lenses and analyze the distribution of refractive index, we proposed Fluorescence Confocal Polarizing Microscopy (FCPM) method for analyzing liquid crystal lenses (LC lenses).

FCPM has wildly been employed in biological research for observation of cells and also used for 3-D imaging of liquid crystal directors. The cells or devices are doped with fluorescent dye which can absorbs the laser light source at the exciting wave length and emit fluorescence at other wavelength. By filtering the exciting light source, the fluorescence signals can be efficiently separated and detected. The signals from the dyes which are anisotropic would be represent the director of LC molecules by the intensity of fluorescence. Therefore, the spatial director of the temporal variation of LC molecules can be calculated. This calculation was finally used to construct the 3-D profile of refractive index and observe the optical properties of the LC lens. Furthermore, the difference between LC lenses driven in convex and concave mode was analyzed by FCPM method, which is difficult to distinguish by fringing pattern.

	$\lvert\Delta\varphi\rvert$	$\Delta\varphi$	LC director	Refractive Index	Ray Tracing
Fringing Pattern	O	X	X	X	X
FCPM	O	O	O	O	O

Table 1-1 Comparison of fringing patterns and FCPM

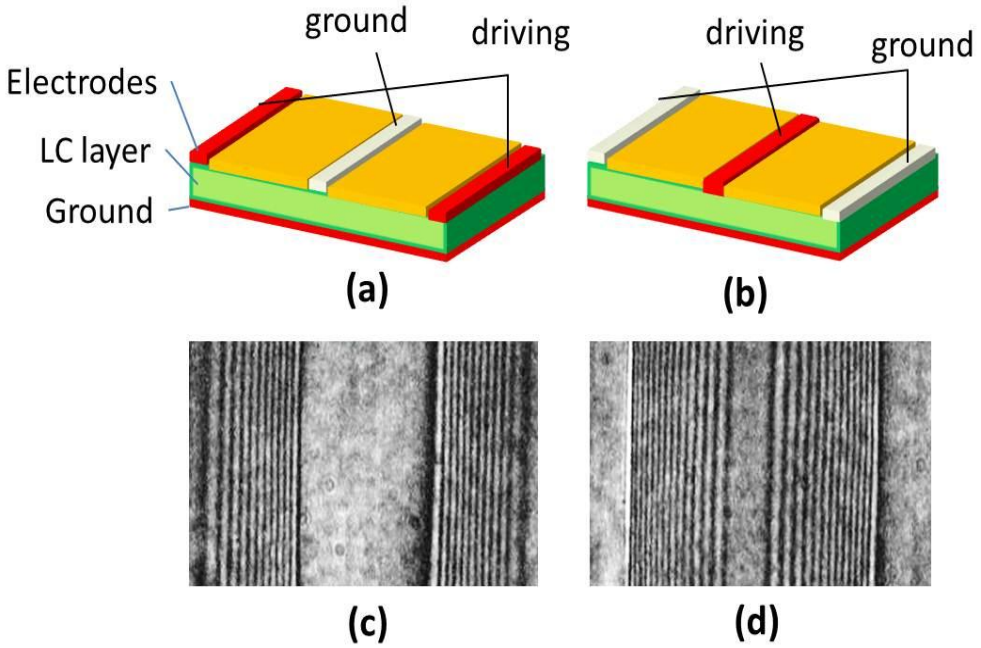

Fig. 1-10 Cylindrical LC lenses driven in (a) convex lens mode and (b) concave lens modes. The fringing patterns of those LC lens modes shown in (c) and (d) individually are very similar and cannot be identified.

1.4 Organization of This Thesis

In this thesis we will concentrate on the fluorescence confocal polarizing microscopy method applied for LC lens analysis. The organization of this thesis is as follows: In chapter 2, some basic principles and theories in LC lens such as the energies in LC cells, the effective focal lengths, and other optical properties will be introduced. In chapter 3, the structures of LC lenses, and the relations between operating voltages and LC lens powers will be clearly presented. In chapter 4, the principle of fluorescence confocal polarizing microscopy method for LC lens analysis will be illustrated, also the experiment setup will be presented simultaneously. In chapter 5, the experiment results and the analysis calculated by FCPM method will be demonstrated, and compared with those by conventional measurement method. Finally, in chapter 6, the conclusion and future works will be given.

Chapter 2

Basic Principles and Theories in LC Lenses

The basic mechanical theories of liquid crystal (LC) molecule and the optical properties will be introduced in this chapter. In mechanical descriptions, the orientation of the LC molecules can be calculated by the total free energy in the LC cell. This energy is induced by the elastic properties of LC material and effects of electric field on LC, as well as the anchoring force on the boundary. To obtain the certain state, the LC molecules will rotate or be bended for the minimized total free energy in the LC cell. In the part of optical properties, the lens effects of LC lenses will be illustrated by the propagations of the plane wave front through the LC lenses.

2.1 Introduction to Liquid Crystals

Liquid crystal (LC) is an intermediate phase between crystalline solid and isotropic liquid. It is believed that LC was discovered in 1888 by Friedrich Reinitzer, an Austrian botanist. He found the phase of LC was changed from a thick and turbid shape to a pure liquid when increasing the temperature. The LC material may flow as liquid, but be oriented as crystal simultaneously in the proper temperature, as shown in Fig. 2-1. At low temperature, the LC material will be in crystal solid state and the molecules will have very high order in position and orientation. However, when the temperature is increased higher than the clearing point, the phase of LC material will change to an isotropic liquid which the position and orientation are totally random. In the isotropic liquid state, the LC material has no birefringence.

According to optical properties, the LC can be classified into five types: nematic phase, smectic phase, chiral phase, blue phase, and discotic phase [25]. The nematic phase LC has the advantage of low viscosity and faster response time. In this thesis,

we chose the Merck nematic LC (E7) which is rod-shaped at room temperature as the main LC material for LC lens application, because that E7 has stable optical and electrical properties at wide temperature range, and it can be easily aligned by an external electric field.

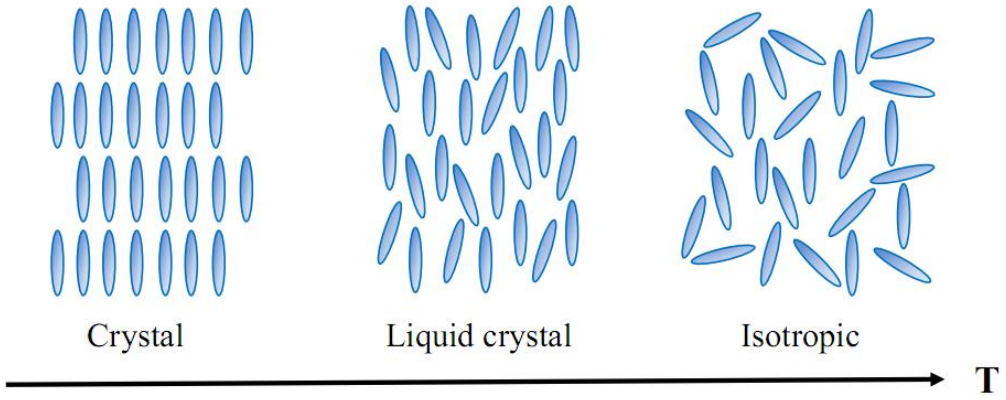

Fig. 2-1 The phase variation of liquid crystal material at different temperature.

2.2 Energies in LC Cells

Without any external energy or boundary condition applied on, the direction of LC molecules is in uniform orientation according to its own material property. If there is external energy or other limited condition like alignment on the substrate, the LC molecules will be rotated or bended to balance the extra forces. This direction and shape change of LC molecules is named deformation (or distortion).

To investigate the deformation of LCs, the continuum theory is recommended regarding that LC is continuous. Therefore, the shape change and direction rotation of LC molecules will be accompanied by restoring forces, which originated from the external fields and boundary conditions. The energies from deformation and the restoring forces are considered as the free energy in the LC lens. Also, the free energy density can be described as the flowing form

$$F_d(\vec{r}) = f_0(\vec{r}) + f_{ela}(\vec{r}) + f_{electric}(\vec{r}) + f_s(\vec{r}) \qquad \text{Eq. 2- 1}$$

where $\vec{r}$ is the LC molecule position, and $F_d(\vec{r})$ represented the free energy density

including the free energy density on uniform state (f_0), elastic energy (f_{ela}), electric and magnetic energy ($f_{electric}$) , and the anchoring effect (f_s).

2.2.1 Elastic Energy

In the nematic phase, the LC molecules are generally regarded as rotationally symmetric ellipsoids, as shown in Fig. 2-2. The unit vector, $\hat{n}$, along the major axis of each ellipsoid is considered as the LC director. In other words, the orientation of the LC molecules can be described with the LC direction, $\hat{n}(\vec{r})$, where $\vec{r}$ is the position of LC molecule. The elastic energy is proposed to describe the spatial variations of LC director $\hat{n}$ which are called splay, twist, and bend deformation. The general definition of the elastic energy is

$$f_{ela} = \frac{1}{2}K_{11}(\nabla \cdot \hat{n})^2 + \frac{1}{2}K_{22}(\hat{n} \cdot \nabla \times \hat{n})^2 + \frac{1}{2}K_{33}(\hat{n} \times \nabla \times \hat{n})^2 \qquad \text{Eq. 2- 2}$$

The above equation is referred to the Oseen-Frank energy, where K_{11}, K_{22}, and K_{33} represent the elastic parameter of splay, twist, and bend deformations of LC material respectively. The terms in the left side are proposed to indicate the free energies of the three possible deformation forms, where the curl and divergence of LC directors are corresponding to different kind distortions of LC director, as shown in Fig. 2-3.

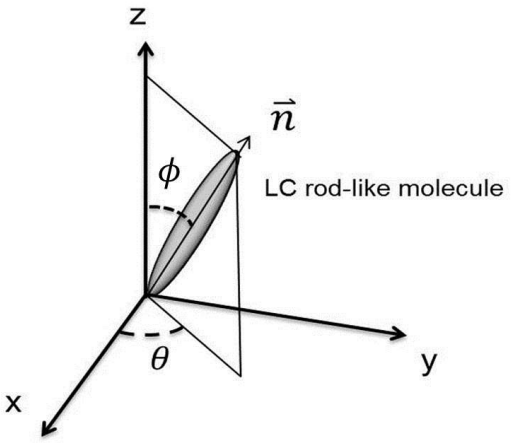

Fig. 2-2 The schematic of rod-like nematic LC molecule. The LC director, $\vec{n}$, indicates the directions of LC molecules in Cartesian coordinate.

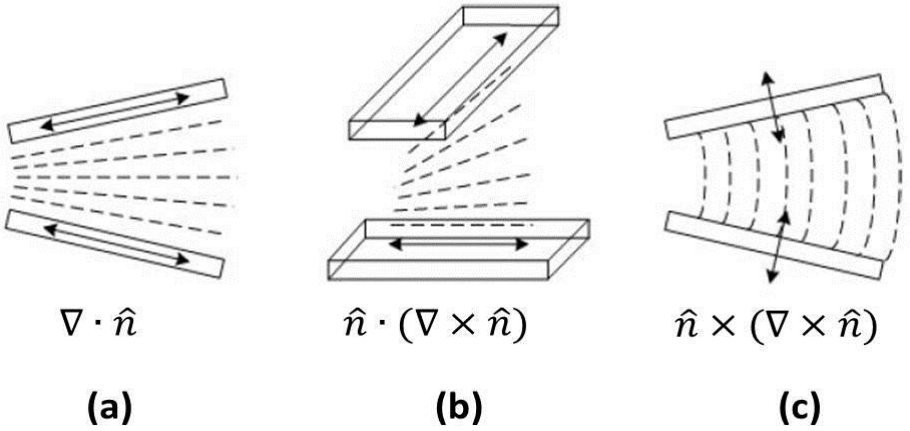

Fig. 2-3 The schematic of three possible deformations: (a) splay, (b) twist, and (c) bend of the nematic LCs.

2.2.2 Electric Field

The electric field is usually considered as external energies to yield the LC directors in specific orientations, as the lens-like shape in this case. Generally, the permittivity of LC molecule in the direction parallel to LC director, $\varepsilon_{\parallel}$, is different from that of perpendicular direction, $\varepsilon_{\perp}$. While an external electric field is applied on the LC lens, there is a torque affecting on the LC molecule which will rotate the director of LC molecule, as shown in Fig. 2-4. In the view of energy, the electric flux density $\vec{D}$ in the LC cells can be expressed as

$$\vec{D} = \varepsilon_{\perp}\vec{E} + (\varepsilon_{\parallel} - \varepsilon_{\perp})(\hat{n} \cdot \vec{E})\hat{n} \qquad \textbf{Eq. 2-3}$$

where $\hat{n}$ is the LC director, and $\vec{E}$ is the electric field in the LC cell. Thus, the electric energy of the LC is derived as following

$$f_{electric} = -\frac{1}{2}\vec{D} \cdot \vec{E} = -\frac{1}{2}(\varepsilon_{\parallel} - \varepsilon_{\perp})\left(\vec{E} \cdot \hat{n}\right)^2 - \frac{1}{2}\varepsilon_{\perp}E^2 \qquad \textbf{Eq. 2-4}$$

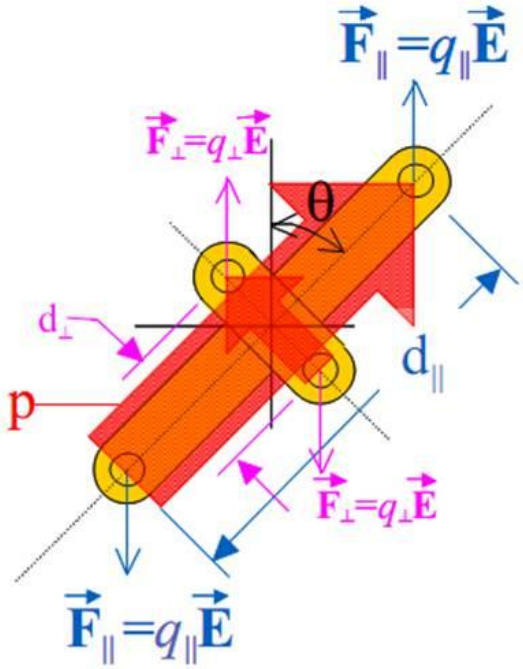

Fig. 2-4 The schematic of the torque induced by the external electric forces on the LC molecule. The LC dipoles on the parallel and perpendicular direction will cause opposite torques which the parallel torque is larger in positive LCs.

2.2.3 Anchoring Effect

In the LC cells, the boundary forces which are usually induced by the alignment layer on the substrates will affect the orientation of LC molecules state. The LC directors are determined along the alignment directions. Thus, the initial LC profile in the LC lens can be yield by the alignment directions of top and bottom substrate.

There are three common alignment types shown in Fig. 2-5, which are the perpendicular, parallel, and anti-parallel alignments. Those alignment methods are utilized for producing the twist-nematic (TN) cells, the π-cells, and the electrically controlled birefringence (ECB) cells respectively. For LC lens applications, generally the ECB alignment cells are adopted for their simplifying control and structures. The energy of the anchoring effect can be described by Rapini-Papoular approach as following:

$$f_s = f_\theta + f_\varphi \qquad \textbf{Eq. 2-5}$$

where

$$f_\theta = \frac{1}{2} W_\theta \sin^2(\theta - \theta_0) \qquad \textbf{Eq. 2-6}$$

$$f_\varphi = \frac{1}{2} W_\varphi \sin^2(\varphi - \varphi_0) \qquad \textbf{Eq. 2-7}$$

θ ,and φ are the polar and azimuthal angles in the spherical coordinate system, as shown in Fig. 2-2, which determine the anchoring effect of two components, f_θ and f_φ respectively. W_θ, and W_φ are the constants depending on the interaction between the alignment layer and the LC molecules. θ_0, and φ_0 are the angles of LC molecules at which the interaction has minimum energy.

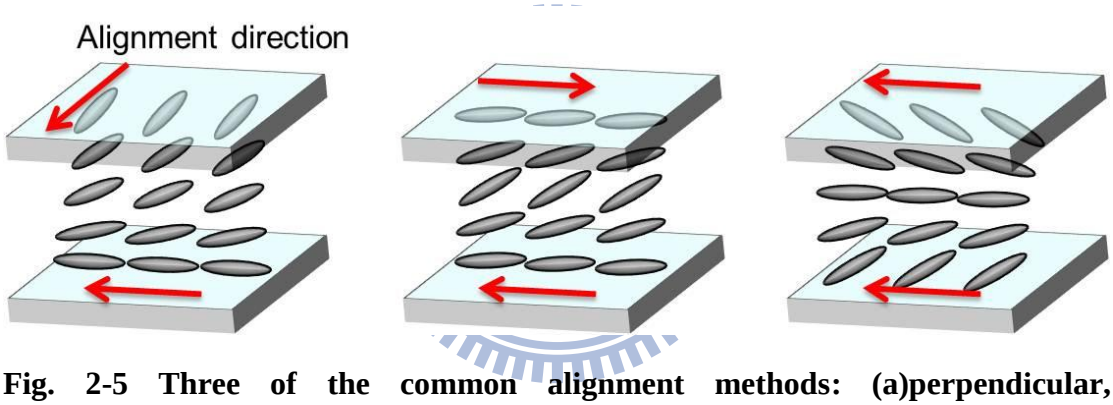

Fig. 2-5 Three of the common alignment methods: (a)perpendicular, (b)anti-parallel, and (c)parallel alignments for LC cells.

2.3 Electrode Configuration & Electrical Field

In this thesis, the nematic LC material E7 from Merck was been employed for the homogeneous LC layer, where the E7 is a positive LC material the whose permittivity difference, $\Delta\varepsilon = \varepsilon_{\parallel} - \varepsilon_{\perp}$, is larger than zero. In other words, the major axis of E7 ellipsoids will be parallel to the direction of electric field $\vec{E}$ when an external electric field is applied on the LC lenses.

However, the LC cells boundary conditions such as the viscosity and the pre-tilt angle of LC molecules will be opposite in polarity to the electric forces.

It is usually complicated to calculate the orientation of LC molecules with the continuum theory, which is considering the equilibrium of restoring forces or free energies in the LC cells. In this thesis, the software electro-optical calculator Display Modeling System (DIMOSTM) developed by Autronic-MELCHERS GmbH was utilized to simulate the fringing field effect and the LC directors with different operating voltages, as shown in Fig. 2-6, the green curves are the potential contours in the dielectric layers and the LC layer. The static and stationary electro-optical response as well as the dynamic behavior of the LC molecules is also be revealed. The three elastic constants (K_{11}, K_{22}, K_{33}), the rotational viscosityγ_1, and the basic parameters of the E7 material are presented in Table. 2-1.

In Fig. 2-6, it is obvious that fringe filed in the regions near to the driving electrodes is stronger than that in the regions distant from the driving electrodes, according to the density of potential contours.

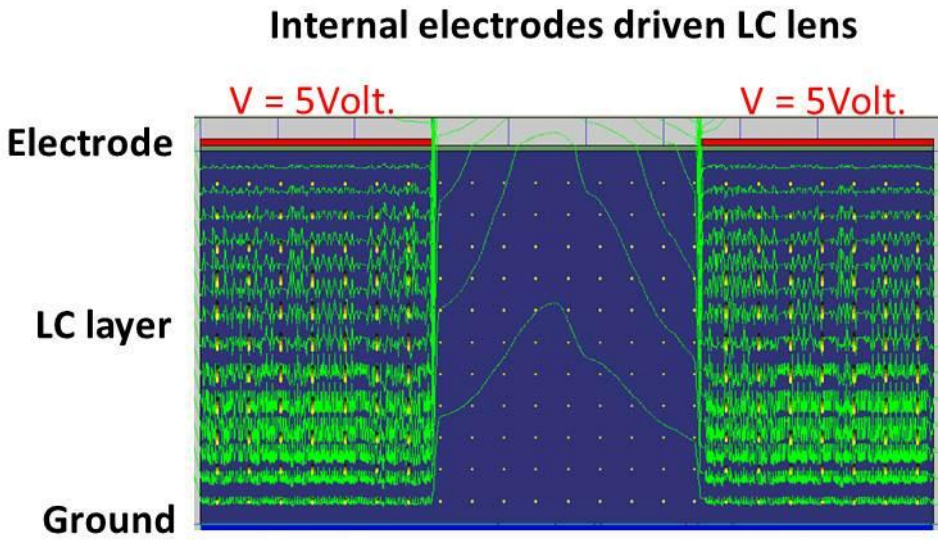

Fig. 2-6 The Simulation of LC lens by 2DiMOS. The controlled electrodes were designed internal the glass substrate, and driven with 5V voltage. The electric field has mostly dissipated from the LC cell.

Items	Specification
Dielectric Constant of Glass Substrate	$\varepsilon_{glass} = 6.9$
The Specification of LC Material (Merck E7)	$K_{11} = 11.1$ pN
	$K_{22} = 5.9$ pN
	$K_{33} = 17.1$ pN
	$\gamma_1 = 233$ m Pa
	$\varepsilon_{\parallel} = 19.28$
	$\varepsilon_{\perp} = 5.21$
	$n_e = 1.7371$
	$n_o = 1.5183$

Table. 2-1 The simulation parameters of LC cells for our proposed LC lens.

2.4 Optical Principle of LC Lenses

LC is a material exhibiting birefringence, which implies that light with different polarization will meet different refractive index while propagating in LC cells. To analyze the birefringence material, the polarization of light usually is decomposed into two eigen-polarizations, where one eigen-polarization is parallel to the optical axis of the material and the other one is on the perpendicular plane to the optical axis, as shown in Fig. 2-7.

The incident light with parallel polarization is named the ordinary light (o-ray), which always meets the ordinary refractive index in the LC cell independent to the incident angle. On the other hand, the refractive index for the extraordinary light (e-ray), whose polarization perpendicular to the optical axis of material, is direction dependent. The refractive index of extraordinary light is varied with the included angle between the incident light and the optical axis of the birefringence material, the

effective index can be calculated by

$$n_{eff}(\theta) = \frac{n_o n_e}{\sqrt{n_o^2 \sin^2\theta + n_e^2 \cos^2\theta}} \qquad \text{Eq. 2- 8}$$

where n_o and n_e are the ordinary and extraordinary refractive index of the birefringence material respectively. θ is the included angle between the incident light and the optical axis, as shown in Fig. 2-8. And n_{eff} is the symbolization of the effective refractive index of the extraordinary light.

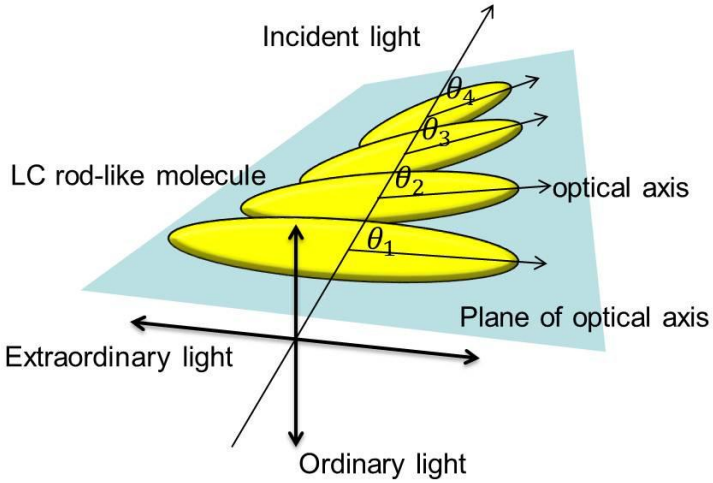

Fig. 2-7 The ordinary and extraordinary lights travelling in the LC material and extraordinary lights see the different indies which are dependent to the included angles between the incident light and the optical axis of LC molecules.

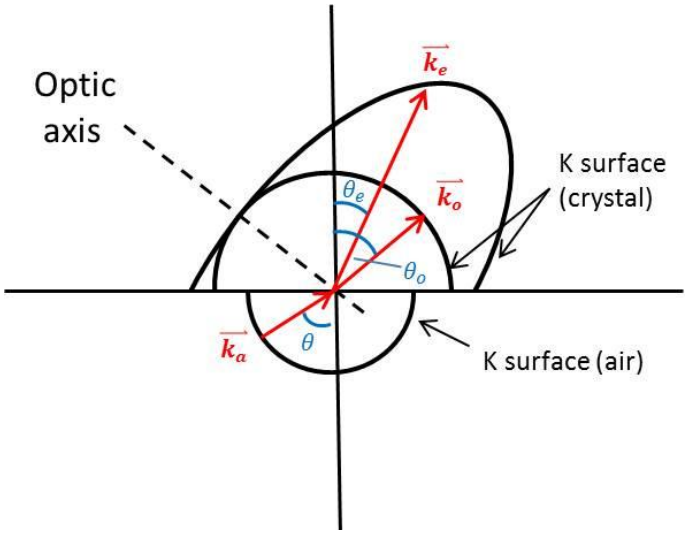

Fig. 2-8 The birefringence of LC material induce that light will mate different refractive index with the included angle between the optical axis.

In the nematic LC lens system, a polarizer will be placed along the alignment direction in front of the LC lens, which will modulate the incident light polarization into extraordinary polarization direction. In other words, the refractive index distribution of the homogeneous LC layer will be varied as the effective index n_{eff}. The lens effect of LC lenses is similar to the GRIN lenses shown in Fig. 2-9 [26]. The refractive index of LC lenses is also gradient distribution from the center to the edge, which is depending on the tilt angles variation of LC molecules as a function of position $\vec{r}$.

To more simply simulate the focusing of LC lens, we consider the incident light as a plane wave propagating through the LC lens straightly. The complex wave front behind the LC lens can be expressed as

$$U(\vec{r}) = A \cdot \exp\left(-j\vec{k} \cdot \vec{r}\right) = A \cdot \exp(-jnk_0 d) \qquad \textbf{Eq. 2-9}$$

where A is the amplitude, $\vec{r}$ is the position, d is the thickness of LC lens, and $k = n \cdot k_0 = n \cdot \frac{2\pi}{\lambda_0}$ is the wave vector of incident light. The index n, which is equal to the effective index n_{eff}, is the function of position $\vec{r}$. The term $-jnk_0 d$ can indicate the phase retardation of the LC lens, and the product of index and lens thickness nd is symbolized to the optical path length (OPL) of the LC cell.

In the thin lens approximation, the complex light wave front behind the LC lens can be expressed as

$$U(\vec{r}) = A \cdot \exp\left(-j\vec{k} \cdot \vec{r}\right) = A' \cdot \exp(jk_0 \frac{r^2}{2f}) \qquad \textbf{Eq. 2-10}$$

where f is the focal length of the thin lens. For the ideal LC lens with fixed thickness d and focal length f, the refractive index distribution should be a parabolic function of position $\vec{r}$. Therefore, the plane wave front will be bended and focused as a parabolic wave when propagated through the LC lens.

Comparing the equations Eq. 2-9 and Eq. 2-10, we can calculate the effective

focal length of the LC lenses by

$$f = \frac{r^2}{2d \cdot \Delta n} = \frac{r^2}{2 \cdot OPD} \qquad \textbf{Eq. 2-11}$$

where f is the focal length, d is the LC layer thickness, and Δn is the refractive index difference between that at the lens center and the position $\vec{r}$. In the right-hand term, OPD symbolizes the optical path difference.

In the other words, it can be consider that the lens effect of LC lenses is achieved by the phase retardation difference on the light wave front propagating over the LC at different position. According to Eq. 2-11, we can calculate the phase retardation function of the LC lens in different lens position is

$$\Delta\varphi(\vec{r}) = \frac{2\pi}{\lambda}(\Delta OPL) = \frac{\pi r^2}{\lambda \cdot f} = c \cdot r^2 \qquad \textbf{Eq. 2-12}$$

where $\Delta\varphi$ is the function of the phase retardation difference between that at the lens center and the position $\vec{r}$. In the right-hand terms, λ is the wave length of the incident light, and $c = \frac{\pi}{\lambda \cdot f}$ is a constant. As Eq. 2-12 illustrates, the phase retardation of the LC lens should be as a parabolic form of the lens position $\vec{r}$.

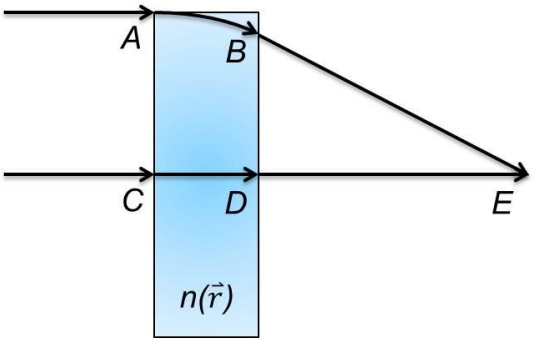

Fig. 2-9 The diagram of that LC lenses can be considered as GRIN lenses for analyzing the focusing light process.

2.5 Summary

The lens effects of LC lenses are achieved by the parabolic optical path difference (OPD), as mentioned in Eq. 2-11, which induced by the effective index $n_{eff}(\theta)$ of LCs. Therefore, generating the smooth gradient orientation of LC molecules is important in LC lens application. Generally, the electrode configuration of patterned electrode LC lenses is on the edge of the LC lens to yield the gradient LC orientation for the convex lens application, as shown in Fig. 1-8. In few cases, the electrode will be patterned at the center while the LC lens is expected to the concave lens applications.

Chapter 3

Electrical and Optical Properties of LC Lenses

In this chapter, the typical fringe-field-controlled LC lens and the gradient drive LC lens (GD-LC lens) will be presented. The most obviously different part between those LC lenses is the electrode configuration design.

While the operating voltage is applied on the electrodes, the LC lenses will be driven with particular effective focal lengths. Usually the larger operating voltage will yield shorter effective focal length. The experiment results of relations between the operating voltages and the effective focal length of LC lens will be illustrated in this chapter. Finally, the fringing patterns and simulation results of the driven LC lenses also will be demonstrated.

3.1. Electrode Configuration Designs

To yield the convex lens effects on nematic LC lenses, the orientation of LC molecules should be modulated into gradient variation, which has been yielded in larger tilt angle on the edge and smaller tilt angle on the center. One method to obtain this orientation is utilizing the fringe electric field from peripheral electrodes, as shown in Fig. 1-8. The other approach is utilized the gradient driven LC lens (GD-LC lens), which modulates the LC orientation by gradient driven voltages with a high resistance material layer functions as electrodes.

3.1.1 Fringe Field Controlled LC Lens

The LC lens operated with fringe field is one of the common LC lens structures. This kind of LC lens is usually with special electrodes patterned on the top glass or other similar material substrates, and uniform planar electrode patterned on the

bottom substrate, as shown in Fig. 3-1 [27].

In this thesis, the nematic LC material E7 was been chosen as the birefringence medium of LC lenses. When the extraordinary light propagates through the LC lens, the wave front will be bended to a parabolic surface form which conforms to the focusing or defocusing property of the LC lens. The phase retardation difference $\Delta\varphi$, or the optical path difference (OPD), which induced by the gradient effective index n_{eff} distribution, will modulate the effective focal length of LC lenses. However, it needs much thicker LC layer to accumulate enough phase retardation difference of LC lens effects which is about 60um thickness, instead of the 5um LC layer in liquid crystal displays (LCDs).

For the convex LC lens application, the gradient orientation of LC molecules is formed by the fringe field which is strong approaching to the peripheral electrodes and weaker at the center of the LC lens. In the ideal LC lens, the effective index n_{eff} should be yielded as the parabolic function of position $\vec{r}$, which will induce the ideal phase retardation conforming to the effective focal length.

To generate a smooth electric field in the LC cell which inducing the ideal phase retardation of the LC lens and improving the lens quality, usually there is a high K material (i.e. the glass) separating the LC layer and the electrodes, as shown in Fig. 3-1. The electrical potential contours of the fringe-field-controlled LC lens with internal or external electrodes are shown in Fig. 3-2. Obviously, the potential contour of the internal electrodes LC lens varies shapely on the edges of electrodes. In those regions, the LC director variation is non-uniform, which will diminish the optical performance of the LC lens.

As mentioned in Eq. 2-11, the effective focal length can be calculated with the phase retardation difference of the LC lens. In the simulation result, it is expectable that the phase retardation distribution of the external patterned electrode LC lens more

approached to the ideal phase retardation function as a parabolic curve.

Furthermore, there is few electric energies has been used in the LC layer of the external electrode LC lens, thus the operating voltage of the fringe-filed-controlled LC lens is unacceptable large. The gradient driven LC lens proposed to solve the issue will be introduced later in this chapter.

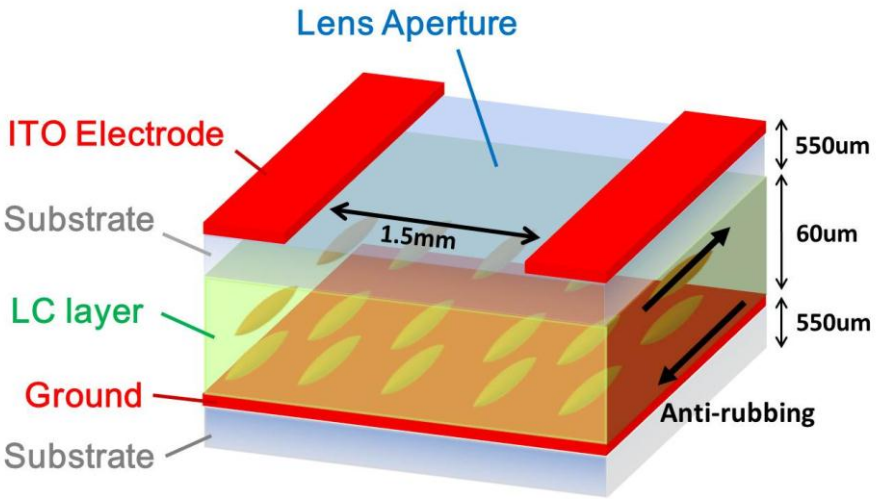

Fig. 3-1 The schematic of cylindrical fringe-field-controlled LC lens with external controlled electrodes which separated from LC layer by the glass substrate to smooth the fringe electric field.

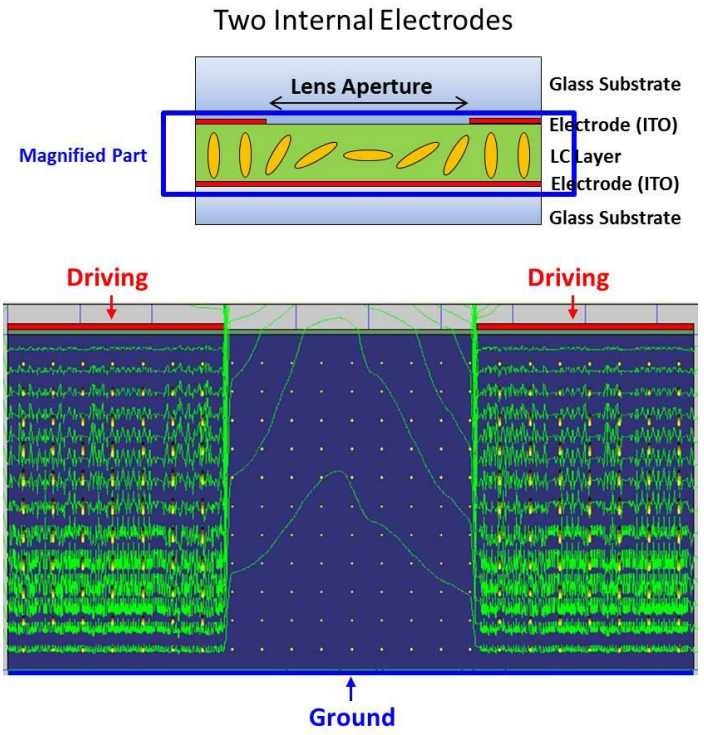

(a)

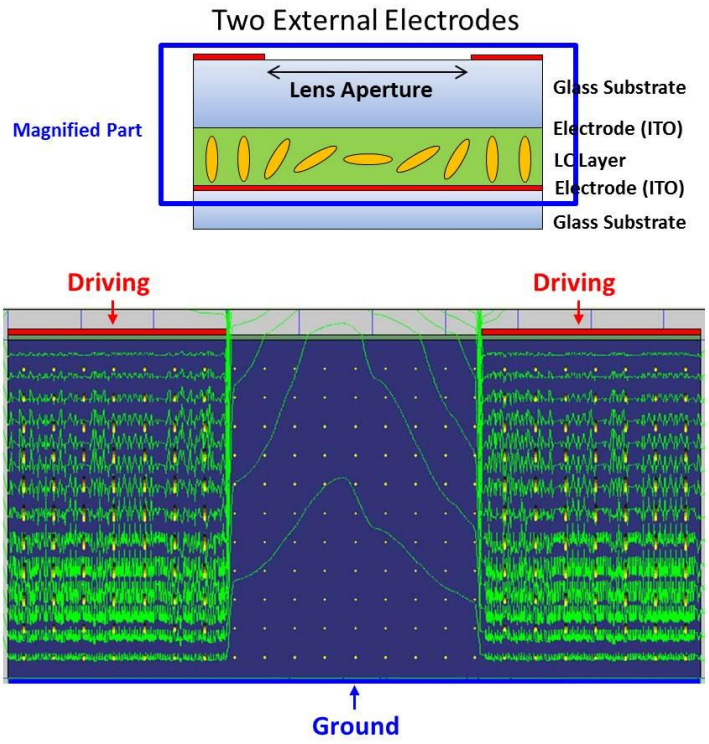

(b)

Fig. 3-2 Simulation of the electric field (potential) of the cylindrical fringe filed controlled LC lens with (a) internal and (b) external parallel electrodes.

3.1.2 Gradient Drive LC Lens

The fringe-field-controlled LC lenses are modulated with the fringe field from the boundary electrodes. Obviously, the potential contour of the internal electrode structure LC lens changed sharply on the edges of electrodes, as shown in Fig. 3-2(a). To generate a smooth electric profile which will improve the lens quality, the electrodes had to be configured outside the glass substrate, as shown in Fig. 3-2 (b). However, the operating voltage of the external electrode structure LC lens is large (about 20Vrms), and the response time longer than 15sec is too slow to the tunable focus lens applications. Thus, the Gradient Driven LC lens (GD-LC lens) as a low operating voltage and fast focusing LC lens with high lens quality was proposed [28, 29].

The conception of the gradient driven voltage applied on LC lenses is coming from the multi-electrode fringe-field-controlled LC lenses, as shown in Fig. 3-3 [30]. The multi-electrode LC lens has high optical performance and is widely controllable by specifically modulating the optimized voltages on each electrode of the LC lens. The homogeneous LC layer and the bottom ITO-glass substrate of GD-LC lenses are the same as the fringe-field-controlled electrode LC lenses. The only difference between those two types of LC lenses is the controlled electrodes on the top substrate. In GD-LC lenses, the multi-electrodes are substituted by the high resistance layer coating between few ITO electrodes, as shown in Fig. 3-4(a). The high resistance material layer is utilized as the internal continuous distribution electrode, which is instead of the high K glass substrate to generate a smooth gradient electric field to yield high quality lens performance.

It is apparent in the simulation results, shown in Fig. 3-5, that most of the electric field is kept in the LC cell, which mostly escapes of the fringe-field-controlled LC

lenses. Thus, lower operating voltage about 5Vrms is needed to drive the GD-LC lens. The focusing response time of GD-LC lens is also largely decreased than the fringe-field-controlled LC lenses whose electrodes are separated by the glass substrate. The response time of the GD-LC lens as shown in Fig. 3-4 can be much reduced to under than 1 sec, with the special over-driven method (OD method) which will be introduced in detail in chapter 5.

Further, it is simply to achieve the convex and concave mode switchable LC lens application with GD-LC lenses, which is difficult with fringe-field-controlled LC lens during the large operating voltage. Those switchable LC lens are well-use in the zoom lens systems. However, there are still some issues in the manufacture process of GD-LC lens, especially the stability of the high resistance layer instead of the multi-electrodes. Thus, in this thesis we will use both of the fringe-field-controlled LC lenses and the GD-LC lenses for analysis.

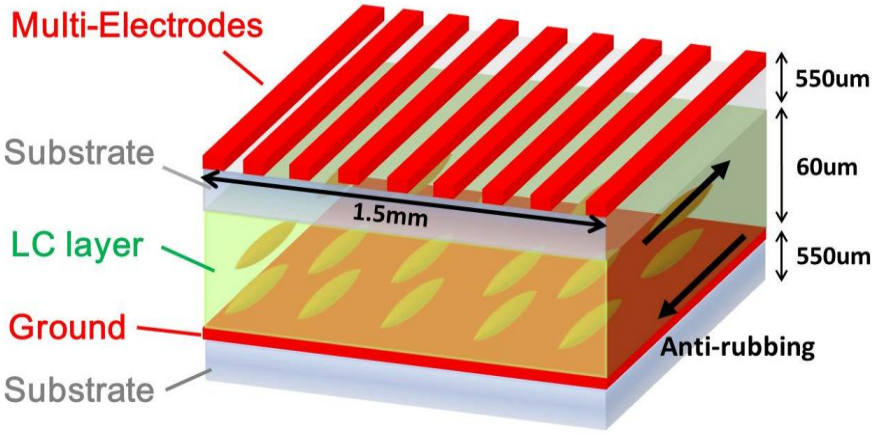

Fig. 3-3 The schematic of the multi-electrode LC lens, where the 9 controlled electrodes were designed with $W_S/W_E = 1$. The multi-electrodes will generate more smoothly gradient electric field comparing to of double-electrodes LC lens.

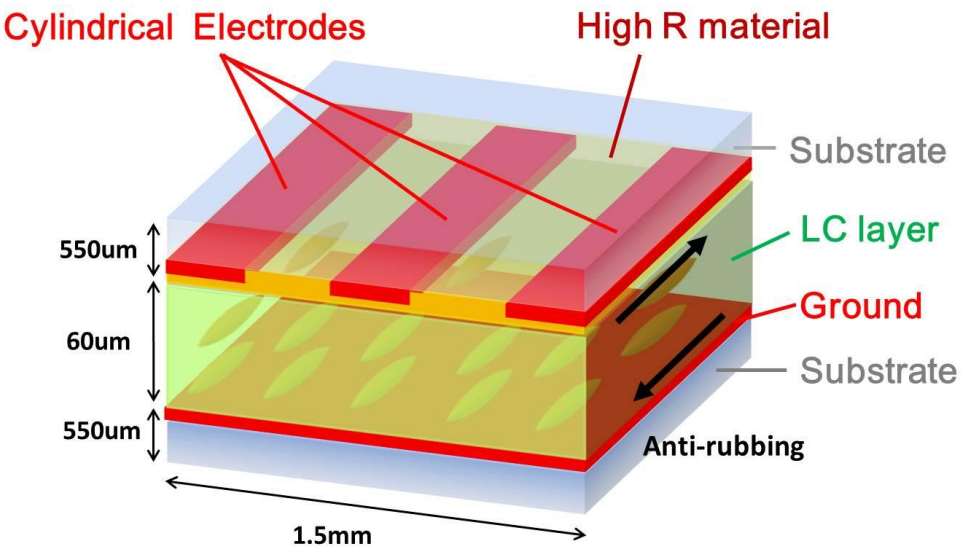

Fig. 3-4 The schematic of cylindrical GD-LC lens. The high resistance layer will modulate the more smoothly gradient varied electric field comparing to the fringe-field-controlled LC lenses.

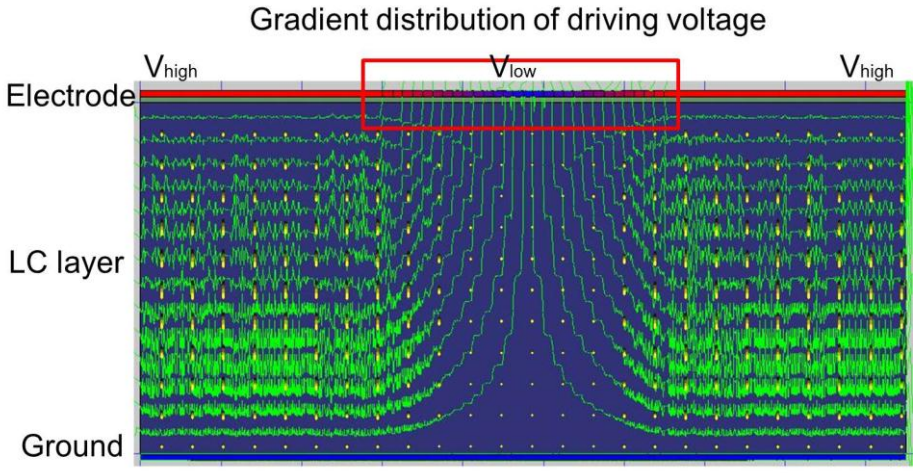

Fig. 3-5 Simulation of GD-LC lens in 2DiMos by continuous multi-electrodes.

3.1.3 Spherical Fringe-field-controlled LC lens and GD-LC lens

For more general lens applications, such as the cameras and glasses, the circular LC lens must be developed. Two kinds of circular LC lenses realized with circular patterned electrode and the controlled high resistance layer GD-LC lens are shown in Fig. 3-6. The principal electrical driven properties of the circular LC lenses are the

same as the cylindrical lenses. Otherwise, the optical properties will be clearly presented later in this chapter.

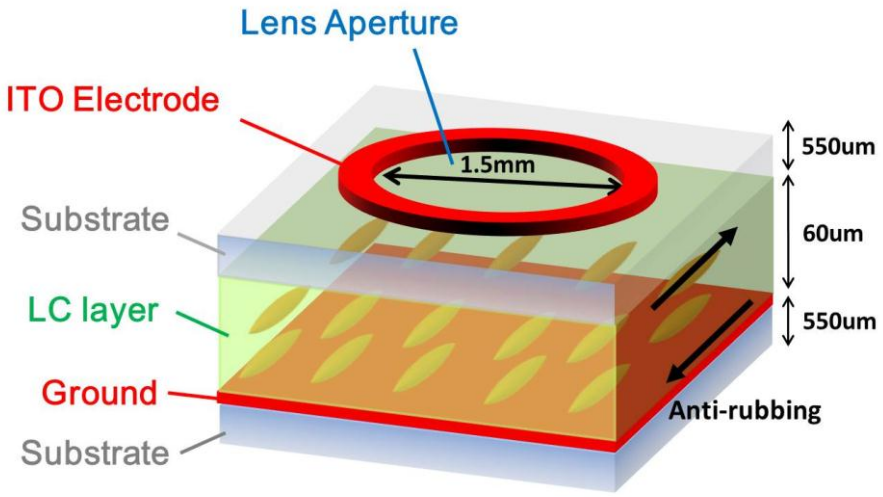

(a)

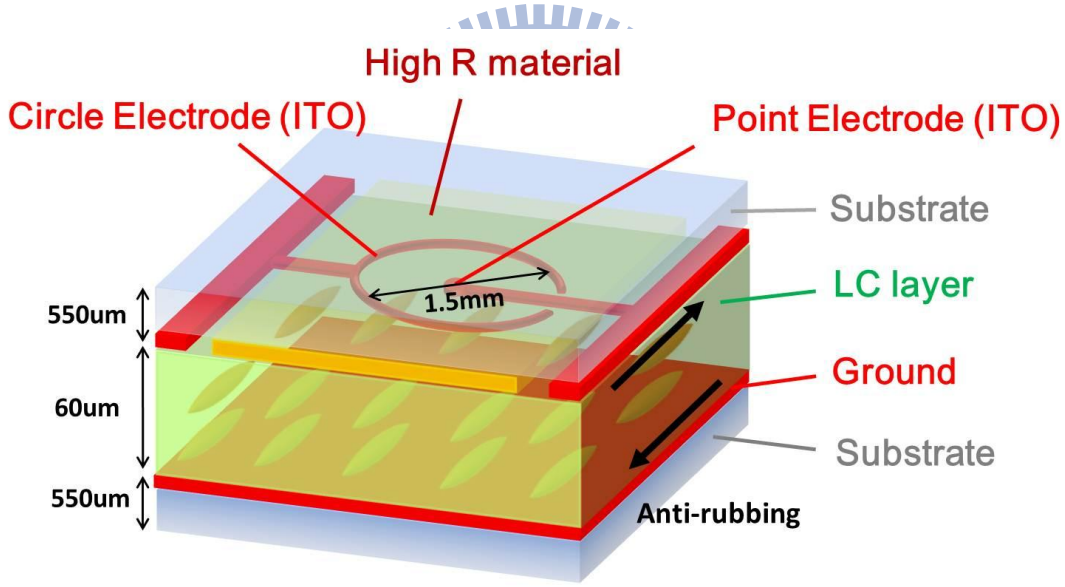

(b)

Fig. 3-6 The structures of (a) the spherical fringe-field-controlled LC lens, and (b) the spherical GD-LC lens (sGD-LC lens).

3.2. Effective Focal Length

The focal length is one of the most important characteristics of a lens element. The effective focal length of the tunable-focus LC lenses can be electrical modulated by adjusting the operating voltages on the controlled electrodes. As illustrated in the preceding sections, larger operating voltage applied on the controlled electrodes will induce larger optical path difference and yield shorter effective focal length.

A simple system to investigate the relation between the effective focal lengths and the operating voltages is shown in Fig. 3-7. The He-Ne laser beam with 632.8 nm wave length is extended by the beam expander, and modulated by the linear polarizer placed in front of the LC lens. The polarizer is arranged parallel to the LC lens alignment. Therefore, the transmitted laser beam has only the polarization component in extraordinary direction of the LC lens. The LC lens will modulate the incident laser beam wither converge or diverge along the optics axis.

For the convex mode LC lens, the GENTEC Beamage Series CCD sensor is arranged behind the LC lens at the focal plane to investigate the focusing profile of LC lens, as shown in Fig. 3-8. While different operating voltages are applied on the controlled electrodes, we can adjust the position of CCD camera to find out the effective focal length of LC lens.

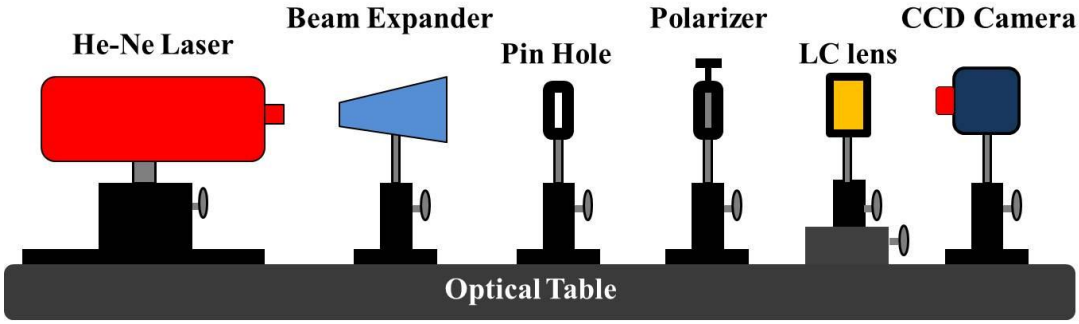

Fig. 3-7 The Schematic of the focal length measurement system.

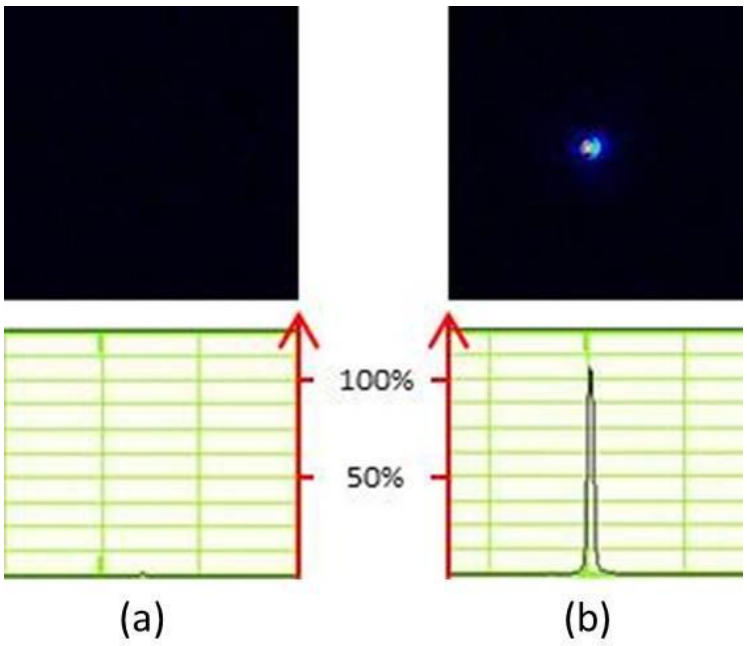

Fig. 3-8 The focusing profile of spherical LC Lens driven at (a) V=0, and (b) V=20V (Vrms) with 1kHz frequency for 5cm focal length.

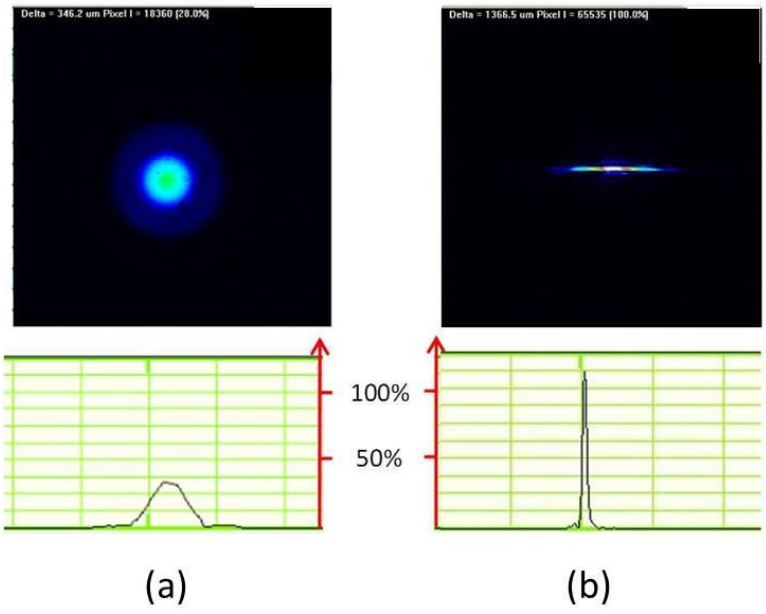

Fig. 3-9 The focusing profile of cylindrical GD-LC Lens driven at (a) V=0, and (b) V=2.35V@2.4kHz for 5cm focal length.

3.3. Fringing Patterns

As it mentioned in chapter 2, the LC lens effect is usually achieved by the optical path difference on the center and the edges of the LC lens. Conventionally, the fringing pattern is utilized to observe the relative phase retardation of LC lenses.

The measure system employs two orthogonal polarizers placed in back and front of LC lens, as shown in Fig. 3-10. While the light is propagating through the LC lens, it will be modulated on the ordinary and extraordinary polarization components with different phase retardations, due to the birefringence of LC molecules. The polarization of the traversing light will be analyzed by the second polarizer and observed by the photo detector. It will detect the minimum light intensity on the photo detector while the phase retardation difference between the ordinary light and the extraordinary light is $(2n+1)\pi$, but maximum light intensity with $2n\pi$ phase retardation difference, where n is an integer.

By plotting the profile of the white-black fringing pattern on the photo detector, the relative phase retardation can be calculated to estimate the optical properties, as shown in Fig. 3-11. The white-black fringing pattern shows dense streaks on the edges but sparse at the center, because the LC lens with unique focal length should have the phase retardation variation as a parabolic function. The parabolic phase retardation variations of the spherical LC lens driven with 20Vrms voltage are calculated by the fringing pattern and the ideal lens formula as Eq. 2-12, and compared in Fig. 3- 12.

However, the fringing patterns only show the relative phase retardation difference which losing the certain values of the optical phase variation in the LC lenses. To investigate the LC directors in detail, the new observing method with Fluorescence Confocal Polarizing Microscopy is proposed in chapter 4.

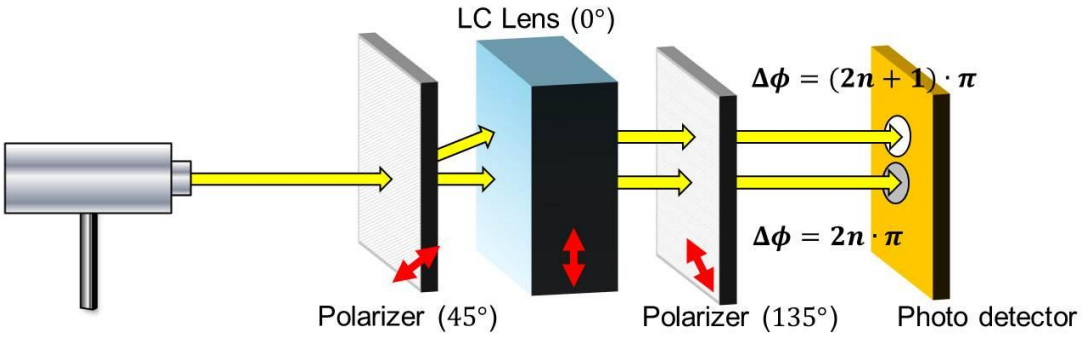

Fig. 3-10 The schematic of the fringing pattern measurement system. This measure system employs two orthogonal polarizers placed in back and front of LC lens, where the phase variation will be detected by the photo detector.

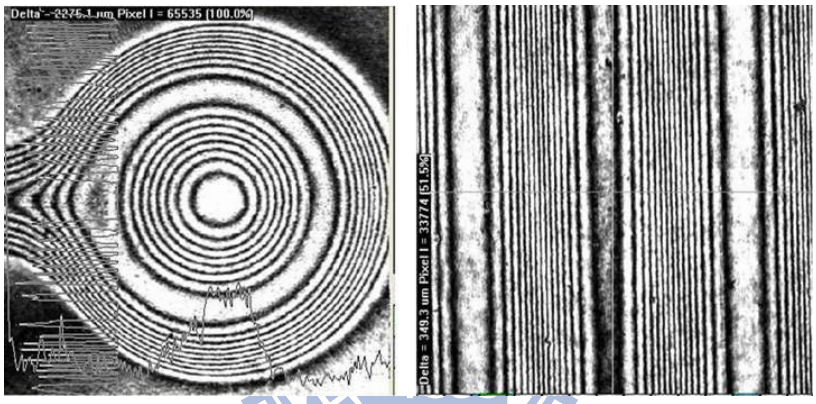

(a) **(b)**

Fig. 3-11 Fringing patterns of (a) spherical (b) cylindrical fringe-field-controlled LC lenses. The phase difference between each two bright stripes is 2π.

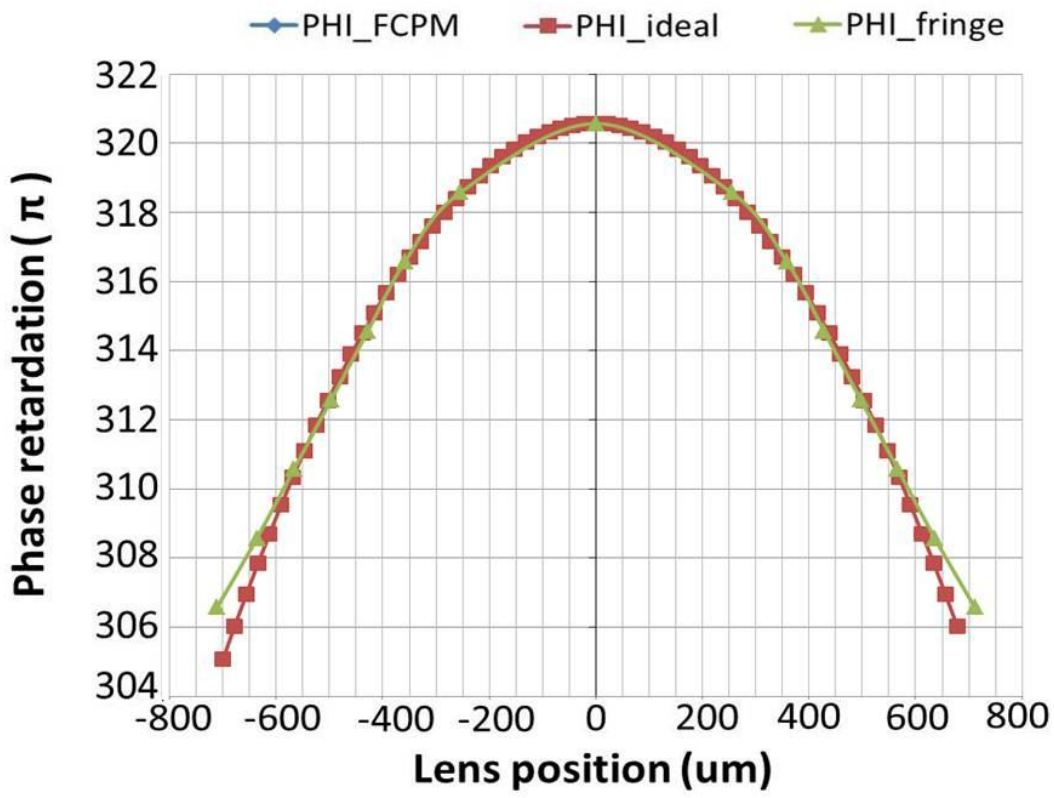

Fig. 3- 12 The phase retardation variation of the spherical LC lens driven with 20V voltage calculated by the fringing pattern. The curve matches the ideal curve by the lens formula in Eq. 2-12.

Chapter 4

Fluorescence Confocal Polarizing Microscopy

The lens effect of the LC lenses is achieved by the phase retardation difference of the LC layer, which is induced with the tilt angle of LC molecules. To investigate the lens performance and other optical properties, conventionally the fringing patterns are utilized to determine the optical path difference (OPD) of the LC lenses. However, fringing pattern can show the integral result of the optical path length through whole the LC layer, but lose the detail information such as the refractive index and the directors of the LC molecules.

In this chapter, the Fluorescence Confocal Polarizing Microscopy (FCPM) method is proposed to observe the molecular orientation inside the LC lenses. The optical properties of LC lenses which are calculated with the LC direction inside the LC cells, such as refractive index distribution, phase retardation, and the effective focal length of LC lenses will be illustrated respectively.

4.1 Fluorescence Confocal Polarizing Microscopy

The Confocal Microscopy (CM) system has been widely employed in biological researches for observation of the biological cells and other microstructures. There is a pair of pinholes in the confocal microscopy system, where one is set behind the light source and the other one is before the photo detector, as shown in Fig. 4-1. The confocal microscopy system allows one to collect light from a very small region, of the sample and thus to optically slice the specimen by scanning the focused beam. The second pinhole will shade the lights emitted from other region. Therefore, the high resolution image of the biological cells will be observed, and the microstructures can be 3D reconstructed by adjusting the focal plane in the vertical direction [31-34].

Fluorescence Confocal Microscopy (FCM) is a version of Confocal Microscopy in which the sample is doped with high-quantum-yield fluorescent dye that strongly absorbs the scanning laser and emits fluorescence light in the other wavelength. The wavelengths variation from the absorbed light and the fluorescent light is called the Stokes shift. If the Stokes shift is sufficiently large that we can separate them by filters, the fluorescence light would be individually determined by the photo detector. Usually, FCM can observe more high-contrast image than the conventional CM system [35-37].

By adding a polarizer in the beam path, the fluorescence emitted from the anisotropic dye molecules will be modulated by the polarizer. Only the polarization component along the linear polarizer can be determined by the photo detector, as shown in Fig. 4-2. Therefore, the Fluorescence Confocal Polarizing Microscopy (FCPM) can visualize the 3D director orientation of the anisotropic media in the samples.

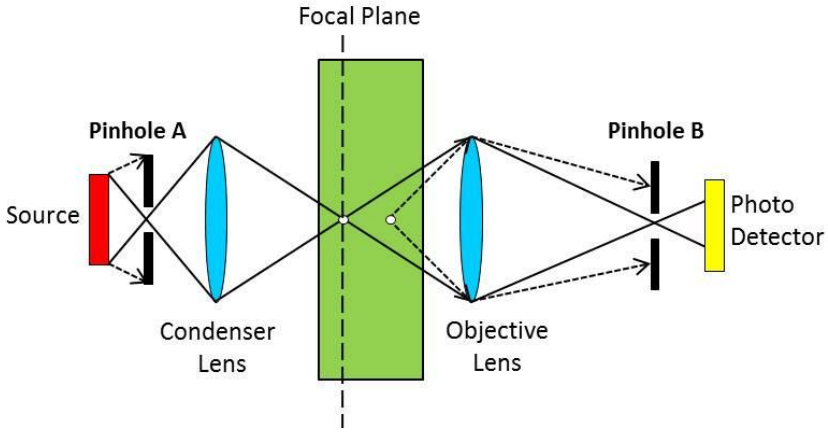

Fig. 4-1 The diagram of transmissive confocal microscopy (CM). Light emitted from the region out of focal plane will be interdicted by the pinhole pair.

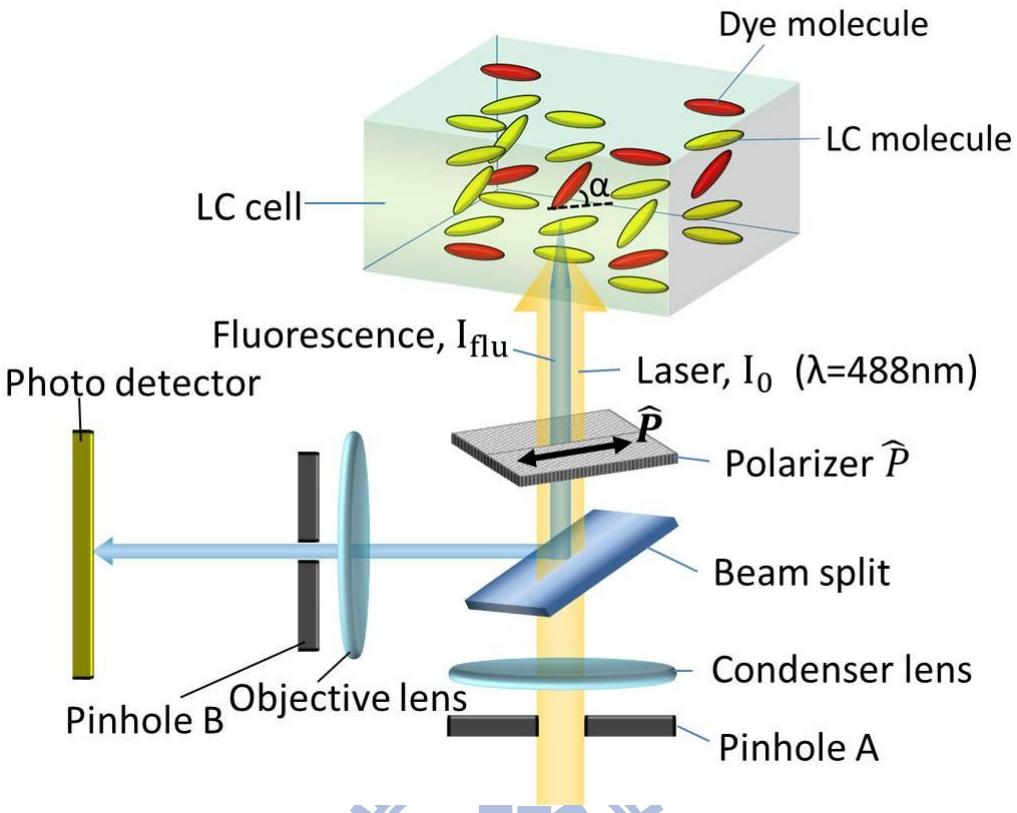

Fig. 4-2 The schematic of Fluorescence Confocal Polarizing Microscopy (FCPM). The scanning laser was emitted from the sample bottom, and fluorescent light intensity of the fluorescence dyes in LC cell will be determined by photo detector.

4.1.1. FCPM Method for LC Lens Analysis

The FV300 Fluorescence Confocal Polarizing Microscopy (FCPM) is utilized to measure the LC directors of the LC lenses. As illustrated in Eq. 2-12, the phase retardation variation of the extraordinary light is modulated by the LC molecule orientation. However, the spatial orientation of the anisotropic liquid crystal (LC) molecules in the LC lens can be indirectly measured by determined the fluorescence intensity from the dye molecules doped in LC lens.

In this thesis, the nematic LC cell has been doped with the fluorescent dye molecules N,N-bis(2,5-di-tert-butylphenyl)-3,3,9,10-perylenedicarboximide (BTBP) which is elongated as the rod-like LC molecules, as shown in Fig. 4-3. The transition

dipoles of both excitation and fluorescence are assumed to be along the long axis of the dye molecule. To image a high contrast 3D director pattern of LCs, it requires small quantity of fluorescent dye with 0.01% by weight [38-40]. As known from studies of the so-called 'guest–host' display modes [41], the anisometric guest dye molecules will be aligned by the nematic host LC molecules in the LC cells. In other words, the directors of the fluorescence dye molecules will be the same as that of the nematic LCs.

The fluorescent light intensity is determined by the orientation of the anisometric dye molecules. For the linearly polarized laser source incident to the LC cell, the probability of a photon absorbed by the fluorescence dye scales as $\cos^2\alpha$, where α is the include angle between the polarization $\hat{p}$, and the direction of the absorption transition dipole, as shown in Fig. 4-4. Similarly, the rate of fluorescence light reaching the photo detector also scales as $\cos^2\alpha$ modulated by the second polarizer. The fluorescence intensity measured by the FCPM can be illustrated as

$$I_{flu} = I_0 \times \cos^4(\alpha) \qquad \textbf{Eq. 4-1}$$

where I_{flu} is the fluorescence intensity and I_0 is the initial intensity of the incident laser source. The rotation and movement of the dye molecules can be ignored because the delay time (also called the life-time of excited state) τ_f of the fluorescence dye is much less than the characteristic time τ_0~10ns of the rotational relaxation of the dye in the LC cells.

The LC lens sample is arranged with the alignment direction parallel to the linear polarizer. Thus, the measured fluorescence intensity with LC lens in un-driven state will be equal to the incident laser source with all LC molecules orientate parallel to the polarization of the scanning laser beam. Therefore, the fluorescence intensity equation can be rewrote as following:

$$\frac{I_{driven}}{I_{un-driven}} = \frac{I_0 \cos^4(\alpha)}{I_0 \cos^4(0)} = \cos^4(\alpha) \qquad \textbf{Eq. 4-2}$$

where I_{driven} and $I_{un-driven}$ are the fluorescent light intensity of the LC lens sample with or without driven voltages measured by the FCPM photo detector.

With the spherical LC lens shown in Fig. 3-6(a), we observed the fluorescent light intensity from each LC layers in driven and un-driven mode. It indicates that the LC directors on the edge are almost perpendicular to the boundary substrate due to the fluorescence intensity is also pale on the periphery regions, as shown in Fig. 4-5. With the polarization direction of the scanning laser and the LC cell alignment are kwon, we can calculate the LC directors orientation in each LC layers, with the include angle α measured by the FCPM.

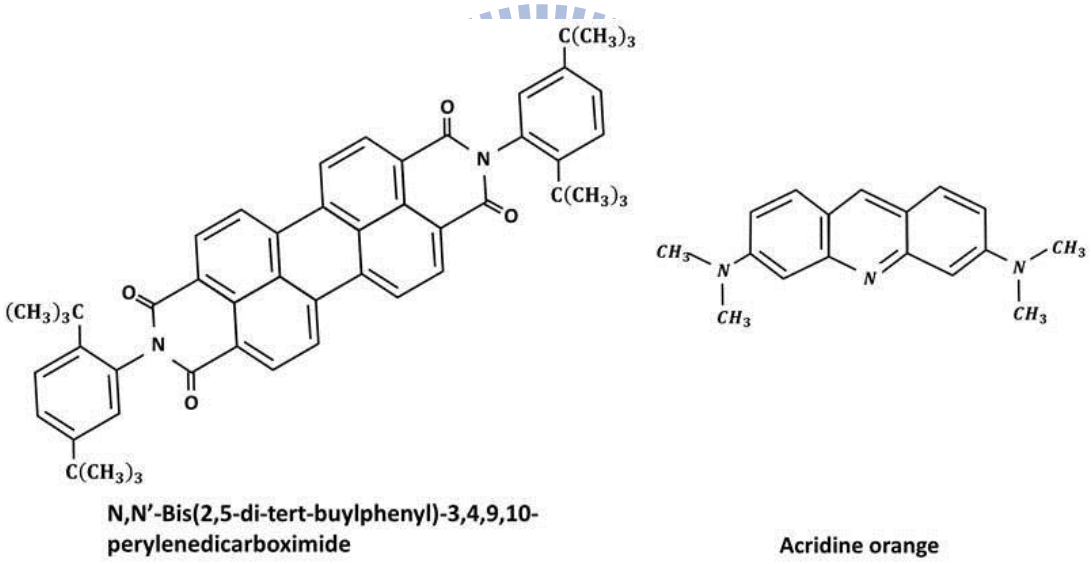

N,N'-Bis(2,5-di-tert-buylphenyl)-3,4,9,10-perylenedicarboximide

Acridine orange

Fig. 4-3 Molecular structures of the fluorescent probes with anisometric shape suitable for FCPM imaging of LCs: BTBP and acridine orange. Both are solvable in thermotropic LCs. When the LC is of a calamitic type (rod-like molecules), the average transition dipole of the dissolved dye molecules is along the LC director.

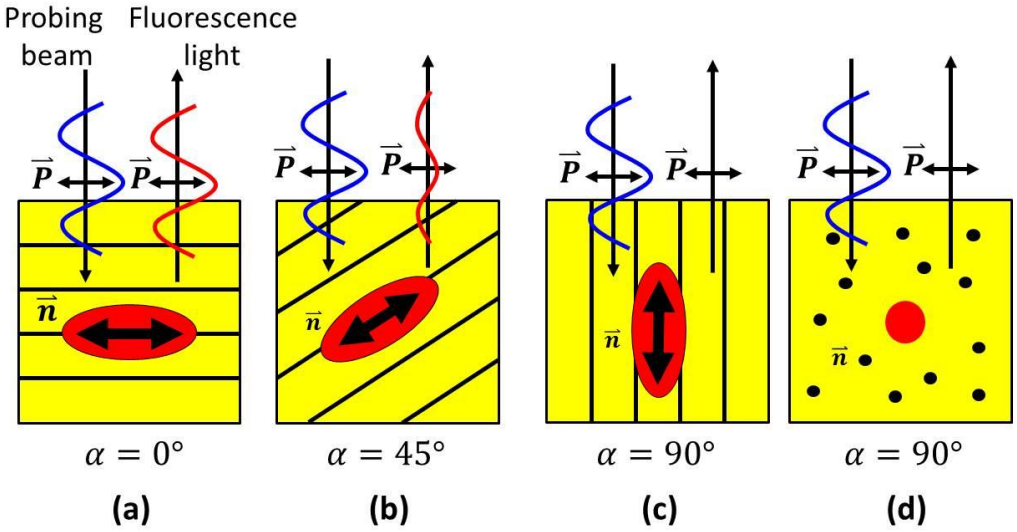

Fig. 4-4 The probability of a photon absorbed by the fluorescence dye scales as$\cos^2\alpha$, where α is the include angle between the polarization $\vec{P}$, and the direction of the fluorescence dyes $\vec{n}$.

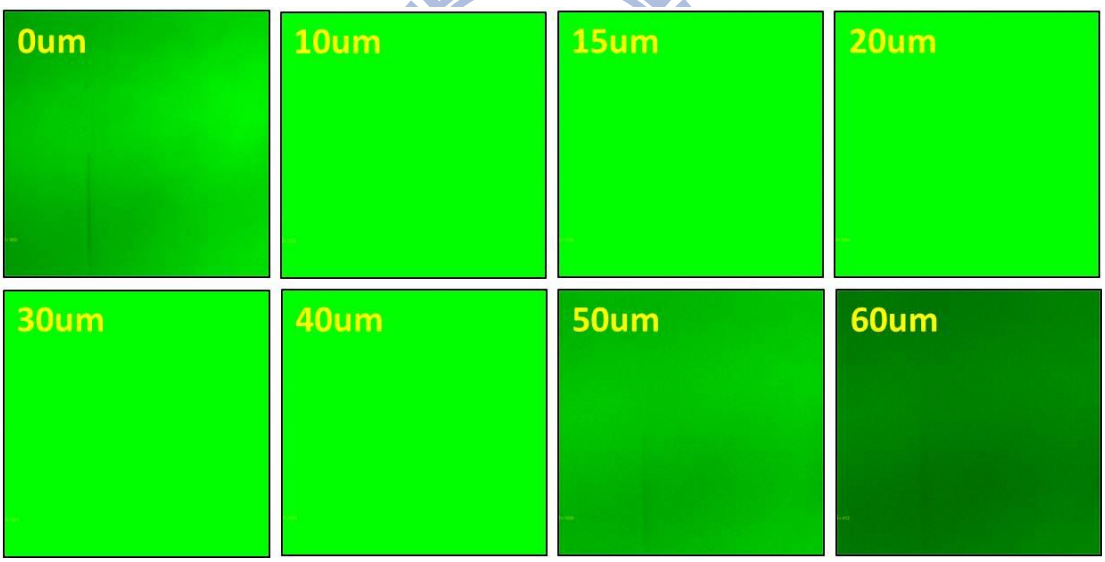

Fig. 4-5 The fluorescent light intensity of each LC layers with no driven voltage.

4.1.2. Exact Intensity of Fluorescence Emission

Ideally, the fluorescent light except from the focal plane should be sheltered by the pinholes. Thus, we can observe the fluorescence of each LC layers and image the 3D director pattern of LC molecules. The resolution of the FCPM equipment is 1um. However, there still is some leaked fluorescent light from other unfocused planes, as

shown in Fig. 4-6. The leaked light is usually considered as the noise signal of the FCPM system which can be eliminated by algorithms.

As shown in Fig. 3-6, the LC molecules and fluorescence dyes are anti-parallel alignment which will generate a uniform distribution of fluorescent light intensity in the initial state. The initial fluorescence intensity distribution function can be described as a rectangular function as shown in Fig. 4-7. The noise signal function of leaked light from adjacent LC layers can be calculated by the anti-convolution with the rectangular initial signal function and the measured fluorescence intensity distribution function. Since the noise signal function has been known, the measurement of the driven LC lens can be consider as the convolution result of the exact signal from the fluorescence dyes and the leaked light from other LC layers, as shown in Eq. 4-3.

$$I_{signal}(z) \otimes f_{noise}(z) = I_{measured}(z) \qquad \text{Eq. 4-3}$$

where I_{signal} and $I_{measured}$ are the exact and the measurement fluorescence intensity from each LC layers by the FCPM scanning. The leaked light noise function is symbolized with f_{noise}, which is modulated by the equipment. By transforming the convolution process to Fourier domain,

$$F\{I_{signal}(z)\} \times F\{f_{noise}(z)\} = F\{I_{measured}(z)\} \qquad \text{Eq. 4-4}$$

$$I_{signal}(z) = F^{-1}\{F\{I_{measured}(z)\} \div F\{f_{noise}(z)\} \qquad \text{Eq. 4-5}$$

the exact fluorescence signal emitted from the focal plane can be calculated. Therefore, we can calculate the LC directors with fluorescence intensity by FCPM.

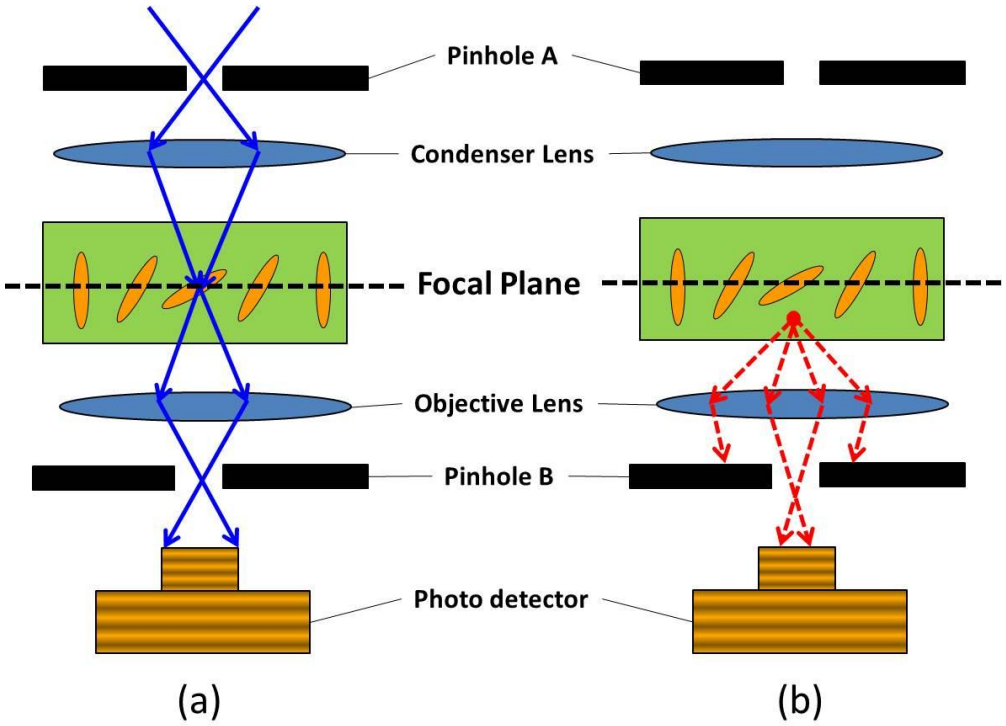

Fig. 4-6 (a) ideally, the fluorescent light from only dyes on focal plane can be determined by the photo detector. (b) However, part of the fluorescent light emitted from regions out of the focal plane will be determined, which can be considered as the noise signal intensity.

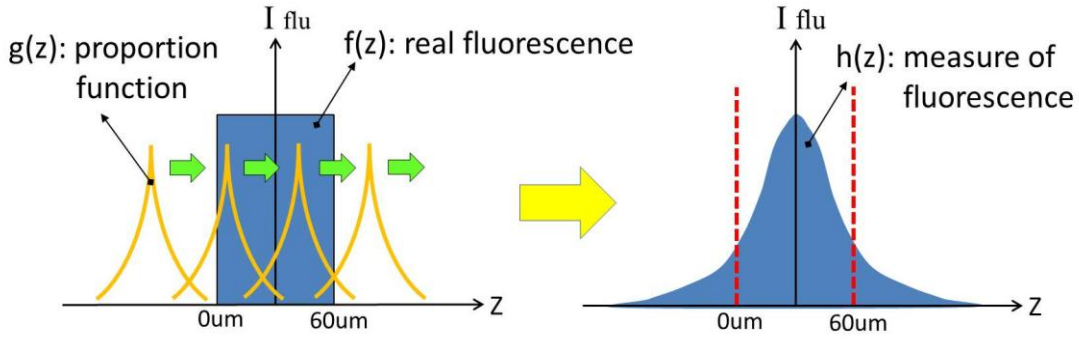

Fig. 4-7 The measurement of fluorescence intensity $h(z)$ can be consider as the convolution of the fluorescence signal function $f(z)$ and the noise signal function of leaked light $g(z)$. The noise signal function $g(z)$ can be calculated by assuming the rectangular initial signal function, and the measurement fluorescence intensity distribution.

4.2 Tilt Angle and Twist Angle

As the LC alignment is anti-parallel, the initial LC molecules orientation is yielding parallel to the laser polarization direction. The spatial variations of LC director $\hat{n}$ with the electric field modulating can be described as the tilt rotation on vertical plane and the twist deformation on the horizontal plane, as shown in Fig. 4-8. Usually, the vertical component of the electric field is stronger than the horizontal component which modulated the twist angle negligible small than the tilt angle. We can simply calculate the 3D director pattern of LC lens with the include angle α, as the laser polarization direction is known.

However, in some cases the LC molecules have deformation both tilt angle and twist angle. To investigate the twist angle of the LC director, we change the laser polarization by 90 degree, as shown in Fig. 4-9, which will modulate the different fluorescence intensity decayed in $\cos^4(\beta)$. The twist angle can be calculated with two include angles α and β in different laser polarizations scanning shown in Fig. 4-9. With the tilt and twist angles, the 3D director pattern of LC molecules can be clearly reconstructed by the FCPM.

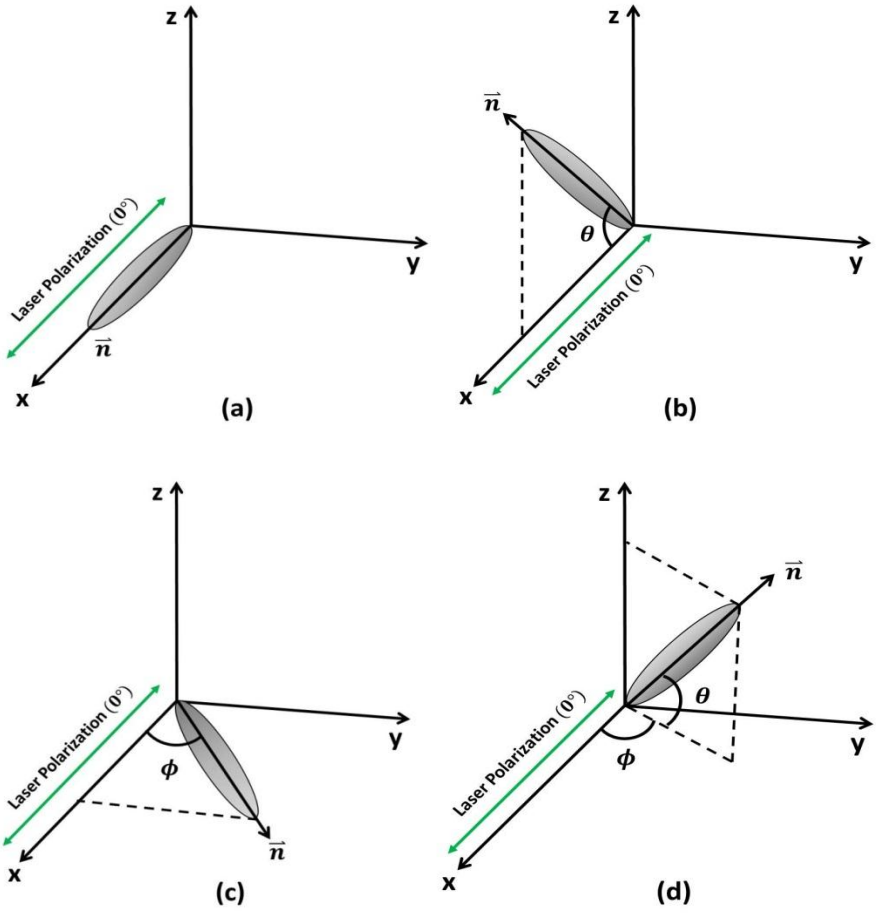

Fig. 4-8 The schematic of rod-like nematic LC molecules in the (a) initial state, and the distortion (b) tilt, (c) twist (c) tilt and twist states. The initial LC director $\vec{n}$ is along the laser polarization on x-axis.

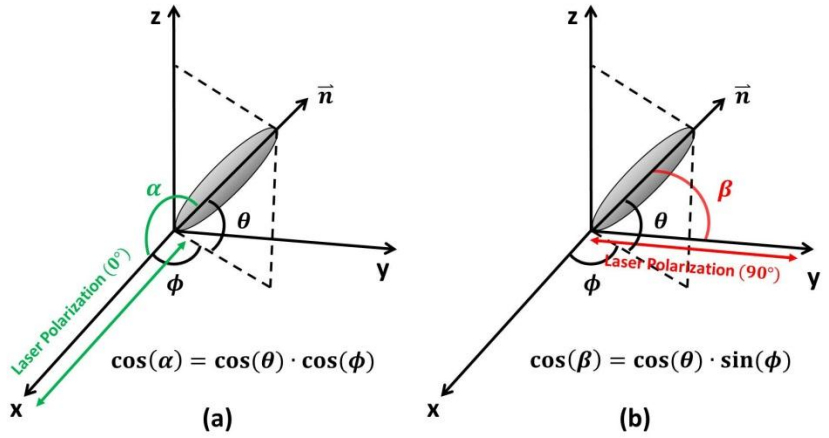

Fig. 4-9 The tilt and twist angle of LC directors can be calculated by modulate the scanning laser polarization which parallel or perpendicular to x-axis, and solve the simultaneous equations from fluorescence intensity decay ration.

Chapter 5

Experiment Results and Discussion

In this chapter, the spherical fringe-field-controlled LC lens and gradient-driven LC lens (GD-LC lens) were both utilized to present the optical properties of LC lenses. The experiment results such as the phase retardation of LC lens measured with the fringing patterns and the FCPM method will be compared and discussed. As shown in Fig. 5-1, the spherical LC lens aperture is 1.5mm and the thickness of the LC layer is 60um. The scanning area of the FCPM is 1.4mm × 1.4mm, and the resolution in vertical direction is 1um.

In the first part, the 3D director patterns and the effective refractive index distribution of the LC molecules measured by the FCPM will be presented. Then, the phase retardation variations of the LC lens calculated by fringing patterns and the FCPM method will be compared. Finally, we will identify the LC lenses in concave and convex lens modes with spatial analysis by the FCPM.

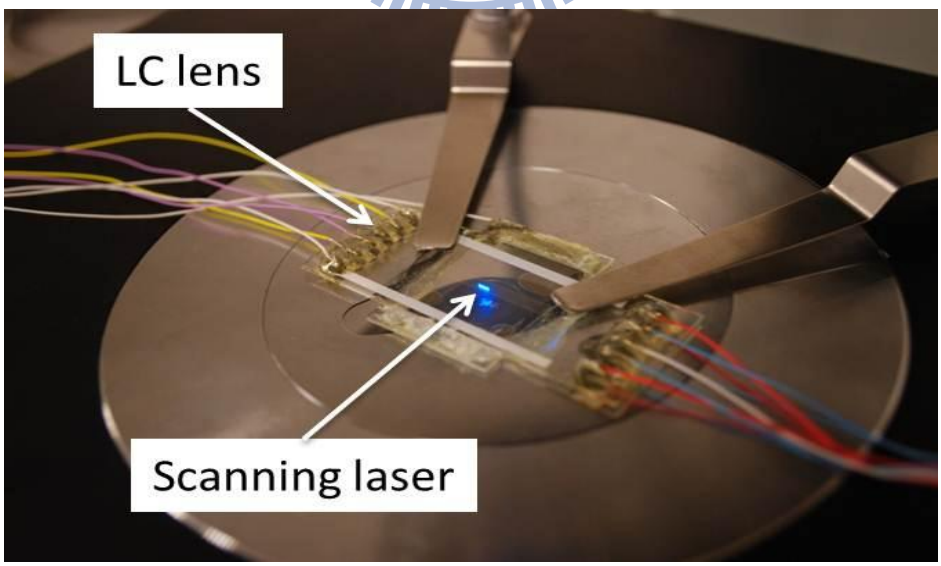

Fig. 5-1 The experiment setup of the measure system with FCPM equipment. The LC lens was scanned by the laser beam emitted from the station bottom.

5.1 Orientation of LC Molecules

The spherical fringe-field-controlled LC lens shown in Fig. 3-6(a) was utilized as the basic LC cell for the analysis. The operating voltages applied on the sphweical controlled electrodes is 20V (Vrms) rectangular wave with 1kHz frequency. The effective focal length of the spherical LC lens was 5cm, which was measured by the focusing intensity as shown in Fig. 3-7. By scanning the fluorescence dyes in the LC cell, The LC directors can be calculated with the initial and driven state fluorescence intensity, as shown in Fig. 5-2. The fluorescence light is strong at the center region and darker on the edge which obviously is induced by the spherical electrode surround the LC lens. The LC molecules in the regions under driven electrodes have been yield with large tilt angle causing the strong vertical electric field. With the filter algorithm and the fluorescence intensity formula in Eq. 4-2, the quotient of the initial and driven state fluorescence intensity is proportional to $\cos^4(\alpha)$, where α is equal to the tilt angle of the LC molecule since the twist deformation is negligible small.

The tilt angle variations of the LC directors in each layer are shown in Fig. 5-3. In order to image the 3-D profile of LC molecules, the rod-like LC modal were used to simulate the tilt angles of each layer according to those contours. The scanning resolution in the vertical direction is 1um. As the contours show, the variance of LC directors is around 20 to 80 degree. The tilt angle of LC molecules under the controlled electrode is larger than that far from the electrode. However, the orientation of LC molecules on the bottom 5um layer is disordered affected by the strong boundary forces of the substrate.

5.2 Effective Refractive Index of LC Molecules

While the extraordinary light traveling in LC lens, the effective refractive index

variation of the LC molecules will modulate the light behavior inside the LC cell. The incident light will be refracted along the direction of gradient index ∇n. The effective refractive index n_{eff} of LC molecules for the extraordinary light is varied with the include angle between the incident light and LC director.

However, it is difficult to measure the LC directors with fringing patterns, the conventional analyzing method, which can just observe the integral result of phase retardation through the LC lens. By using the FCPM method, the exact effective index $n_{eff}(\alpha)$ can be easily calculated with the birefringence formula in Eq. 2- 8, as the LC molecules tilt angle distribution has been measured by the fluorescent light intensity decay rate. In this LC lens structure, the included angle α between the laser polarization and the LC director is approximate to LC molecules tilt angle θ, as the LC lens alignment is parallel to the laser polarization direction and the external electric field is on the vertical direction of the LC lens transection.

By scanning the LC cell with FCPM, the refractive index distribution of each LC layers can be calculated and plotted as Fig. 5-4. The scanning range is about $1.4\text{mm} \times 1.4\text{mm}$. The effective index of LC medium n_{eff} will be modulated between $n_o = 1.7472$ and $n_e = 1.7472$ for the birefringence material E7. As the contours show, the index distribution of each layer is around 1.74 to 1.58. The index variation Δn is only 1.6, which is not achieving the maximum $\Delta n_{max} = n_e - n_o \cong 0.22$ of E7 material due to the deformation of the LCs at the lens center and not vertical tilt angle of LCs at the border. Actually, the maximum index variation Δn_{max} is difficult to be achieved with fringe-field-controlled LC lens structure. Therefore, the cell gap of LC layer is usually thicker, assuming the high optical power is required. The contours are more broken in the top and bottom layers which are both closed to the boundaries, while the middle layers have more smooth distribution.

The contours of LC effective index distribution are shown as some concentric

circles, which are induced by the symmetrical electric field from the spherical controlled electrode on the top substrate. While the light travels through the LC layers, it will induce the spherically gradient-varied optical path difference (OPD) as it traveling through a conventional lens which has different thickness at the center and at the border. The phase retardation variation of LC lens calculated by the FCPM and the fringing pattern will be shown in next section.

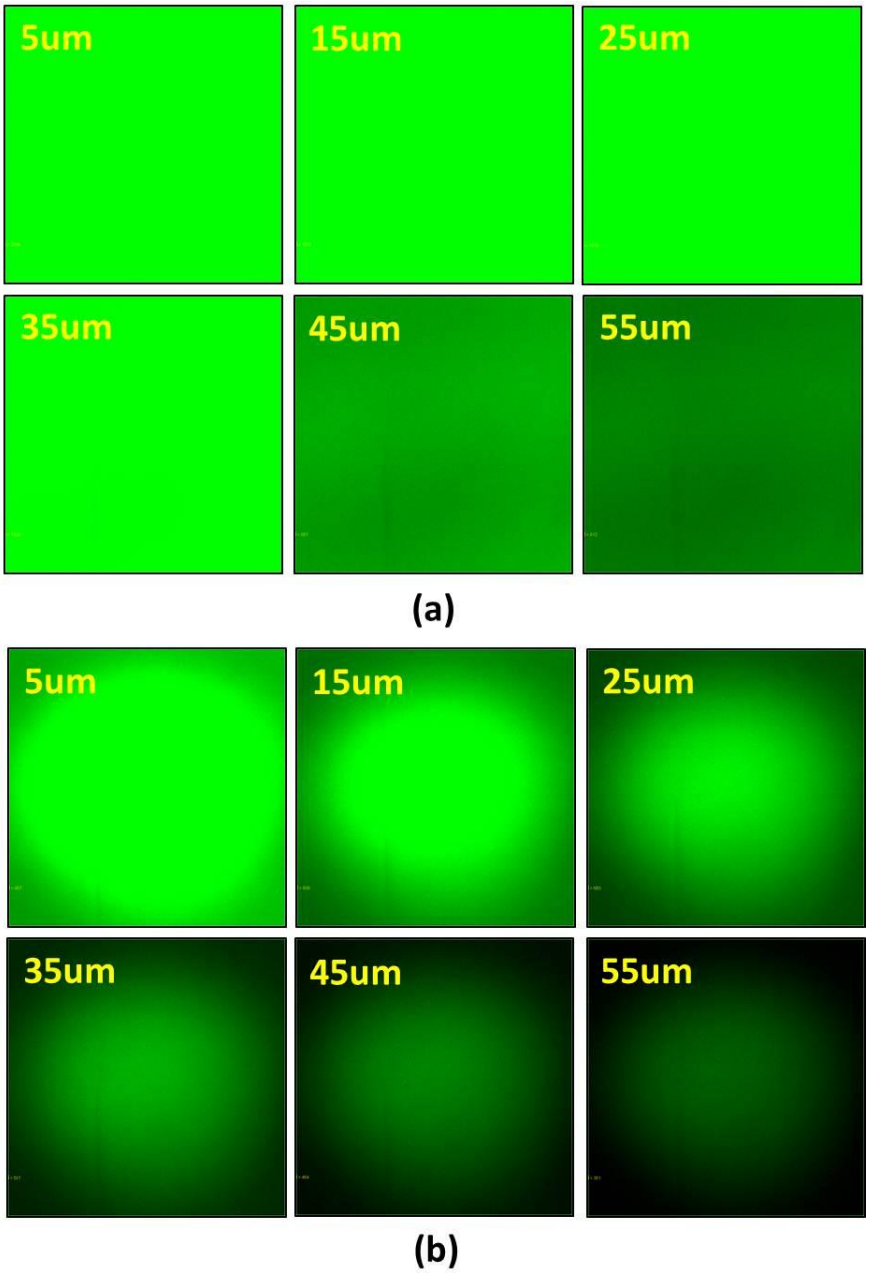

Fig. 5-2 The fluorescent light intensity measured by FCPM of the spherical LC lens with voltage (a) $V = 0$, and (b) $V = 20$volt for 5cm focal length.

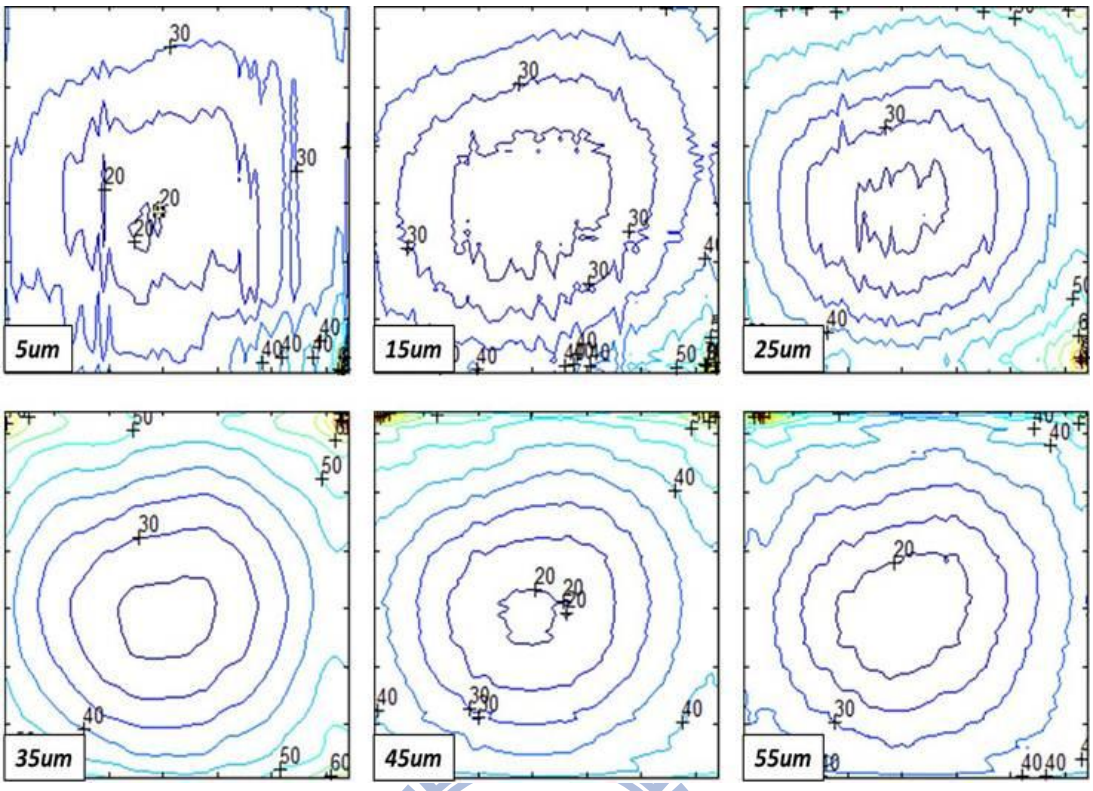

Fig. 5-3 Contours of the LC tilt angle distribution of each LC layers.

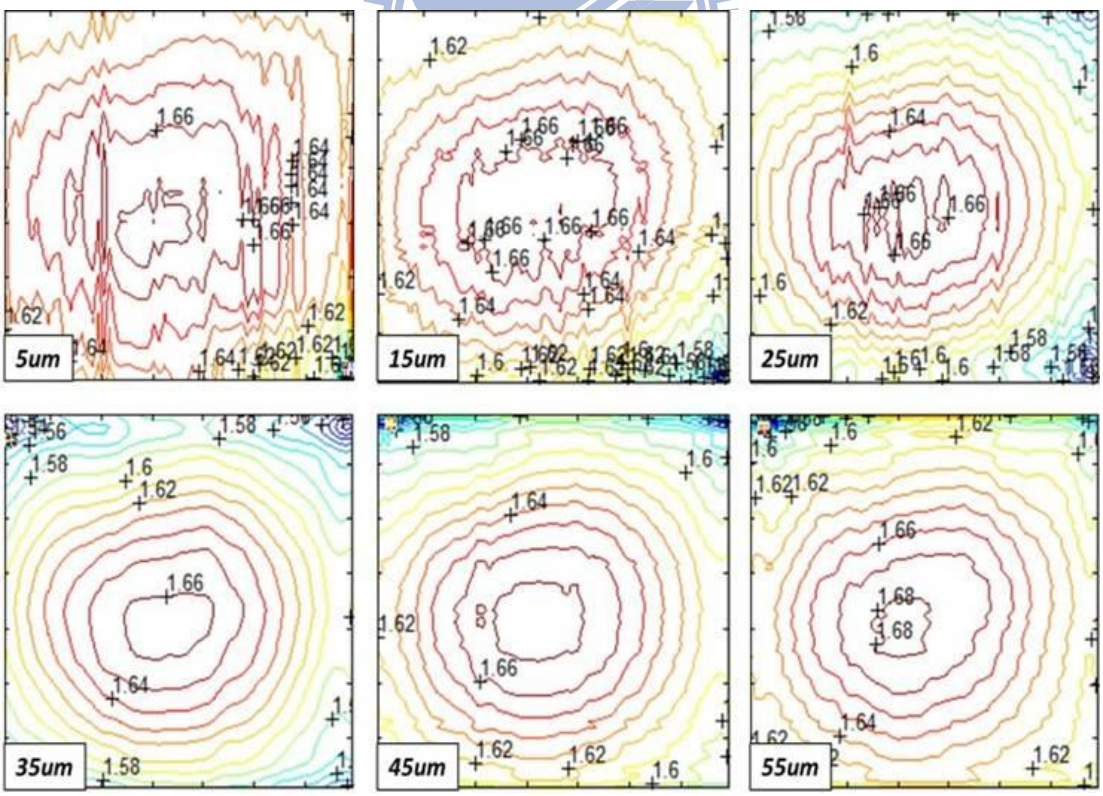

Fig. 5-4 Contours of the refractive index of each LC layers.

5.3 Phase Retardation Variation of LC Lenses

To verify demonstrate the optical properties of the scanning results, the first order optics of LC lens is illustrated by calculating the phase retardation φ. Typically, the f-number (f/#) of LC lens is relative large compared to the conventional lenses. Thus, paraxial approximation can be employed for the propagation of rays in LC lenses to calculate the phase retardation. If we assume light traveling straightly through the LC lens, the phase retardation of the LC lens in Fig. 5-1 can be approximated to

$$\varphi = \frac{2\pi}{\lambda} \cdot \int n(\vec{r})\, ds = \frac{2\pi}{\lambda} \cdot \int_0^d n_{eff}(x, y, z) dz \qquad \textbf{Eq. 5-1}$$

where d is thickness of the LC layer, and λ is wavelength of the incident light. Optic axis of the LC lens was set to be along z-axis. From Eq. 5-2, the integral result of phase retardation from 0um to 60um LC layer was calculated, shown in Fig. 5-6. Fig. 5-6 clearly indicated the phase retardation at the center of the lens was around 371π, and the exact phase difference between the center and border was around +12π. The relative phase was also measured by fringing pattern method, as shown in Fig. 5-7. Within the scanning area, the relative phase difference was also around 12π, but the signs cannot be directly evaluated.

To compare the accuracy of measured results, focal length corresponding to the phase retardations was investigated. Under the 20V (Vrms) driving voltage, the LC lens had maximum focal intensity at 5cm distance away from the lens when illuminated by a laser source (λ = 632.8nm). The ideal distribution of relative phase retardation $\Delta\varphi(\vec{r})$, for LC lenses with focal length f, can be represented by following equation:

$$\Delta\varphi(\vec{r}) = -\frac{2\pi}{\lambda}\left(\frac{r^2}{2f}\right) \qquad \textbf{Eq. 5-2}$$

where r is aperture ray height in cylindrical coordinate system. Eq. 5-2 indicates the

form of the phase retardation $\Delta\varphi(\vec{r})$, is a parabolic curve if no spherical aberration occurs. Compare the results by capturing the cross section of profiles in Fig. 5-6 and Fig. 5-7, the curves, as well as the ideal parabolic curve for 5cm focal length, are shown in Fig. 5-8. These three curves are almost matched indicates the measured results of FCPM method and fringing pattern were coherent, and also matched with the measurement of focal length. The caparison of three phase retardation variations shows that the LC lens can modulate light as the conventional lenses.

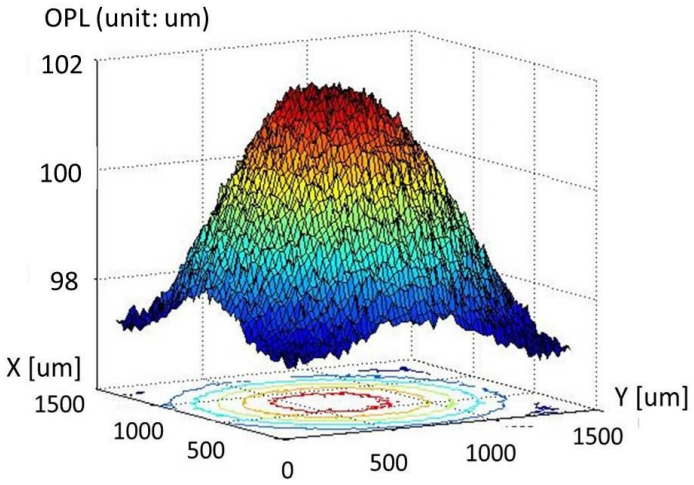

Fig. 5-5 The optical path length of spherical LC lens driven in 20V (Vrms), for 5cm focal length, measured by the FCPM method.

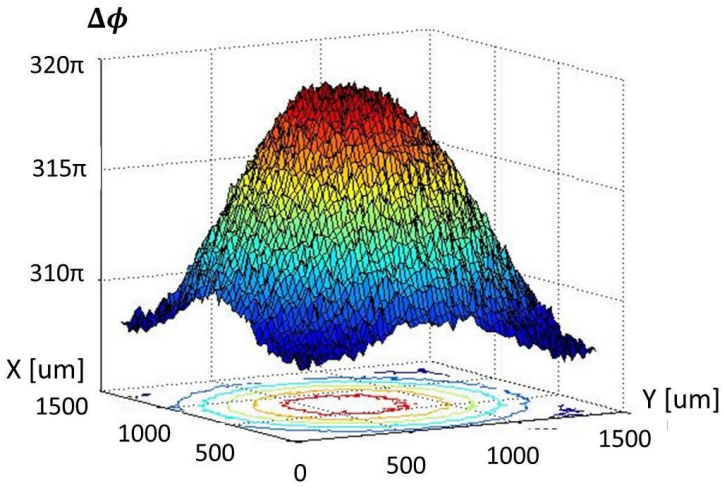

Fig. 5-6 The phase retardation of spherical LC lens driven in 20V (Vrms), for 5cm focal length, measured by the FCPM method.

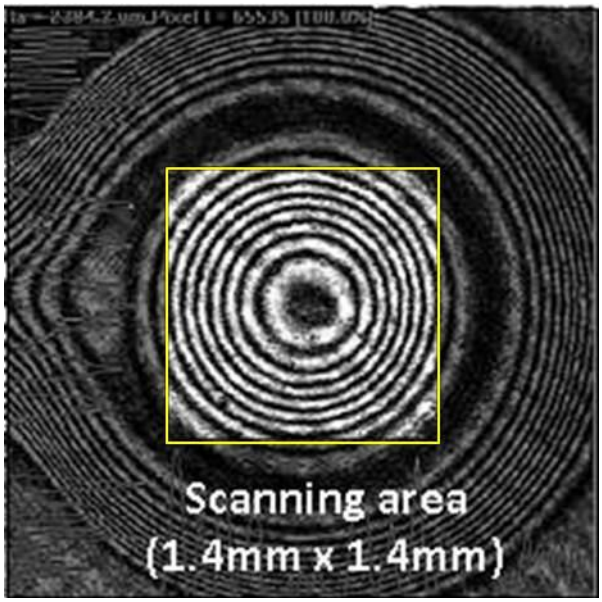

Fig. 5-7 Fringing Pattern of the spherical LC lens driven in 20V (Vrms)

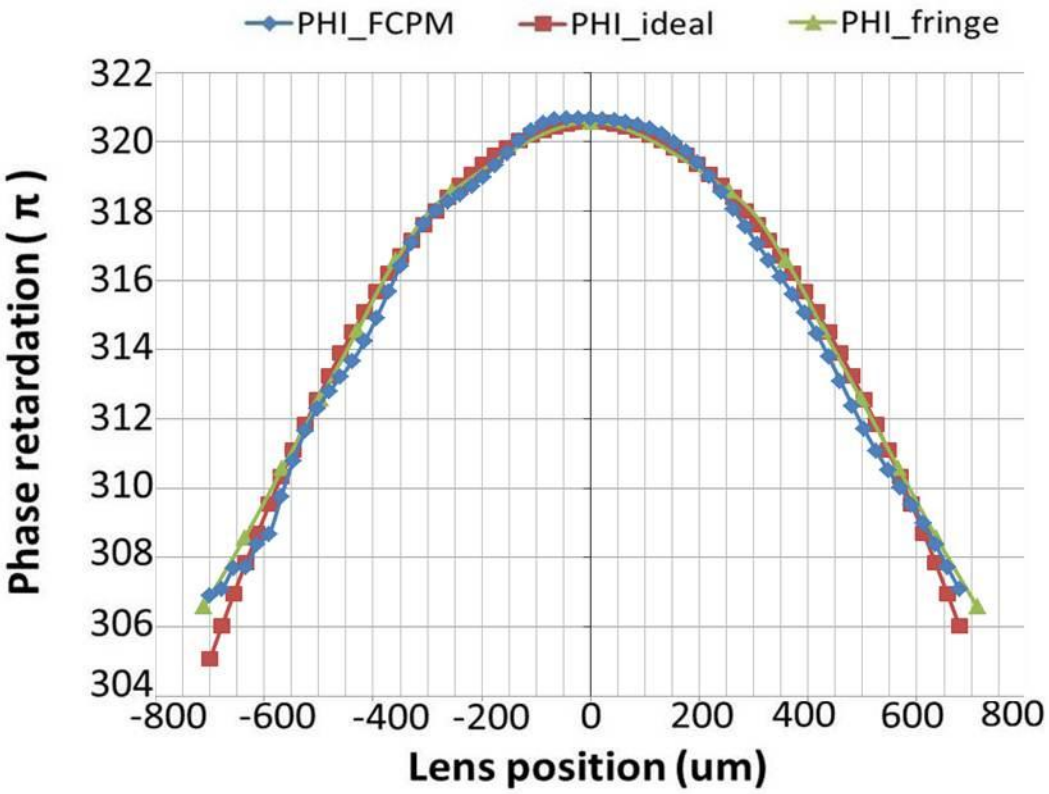

Fig. 5-8 The phase retardation variation of the spherical fringe-field-controlled LC lens driven with 5V voltage, which were calculated by the ideal lens formula shown in red curve, the fringing pattern result in green curve, and by the FCPM method in blue curve.

5.4 Convex and Concave Modes of LC Lenses

The primary difference between the FCPM method and the fringing pattern is that the FCPM can illustrate the exact phase retardation of LC lens, not only the relative phase difference as fringing pattern. For instance, when a light travels through a convergent or a divergent LC lens with the same focal length, the fringing patterns will seem the same; however, the FCPM could identify the difference clearly.

To demonstrate the investigated phase retardation measured by FCPM method, the spherical gradient driven LC lenses (sGD-LC lenses) were utilized to demonstrate the convergent and divergent LC lenses, or called as convex and concave LC lens modes [42]. As shown in Fig. 5-9(a), while the driving voltage applied on the outside electrode and ground on the center spot electrode, the sGD-LC lens can collect the incident lights as a convex lens. The LC molecules were modulated with lager tilt angle at the border due to the electric field from spherical electrode, as shown in Fig. 5-10(a). This orientation of LC molecules will modulate the effective index of LC molecule is approaching to the ordinary index n_o at the border, while it is approximated to extraordinary index n_e in the center region of LC lens. Oppositely, the LC directors at the border were almost parallel to the alignment in concave lens mode with the driven voltage applied on the spot electrode at the lens center and ground on the spherical electrode as shown in Fig. 5-9(b).

As shown in Fig. 5-11, the fringing patterns of sGD-LC lens in convex and concave modes are similar, though the optical properties of two modes LC lenses are much different. It is difficult to identify the LC lens optical properties, which converging or diverging lights, with fringing patterns whose bright-dark stripes show only the absolute value of phase difference of LC lens.

However, the exact phase retardation results calculated by the FCPM method in

Fig. 5-12 show the difference of the two LC lens modes clearly. In convex lens mode, the optical phase at the border was slower than that at the center, because the effective index of LC molecules was lager at the border region which was under the driven spherical electrode. In other hands, the opposite LC orientation driven in concave lens mode would induce the optical phase as a concave surface which the phase at the border was faster than at the center.

With the exact phase retardation calculated by the FCPM, we can investigate the light behavior in detail while it traveling through the LC lens. The lens effects of LC lenses can be consider as the gradient-index lens (GRIN lens) systems with the effective index distribution has been measured by the FCPM method.

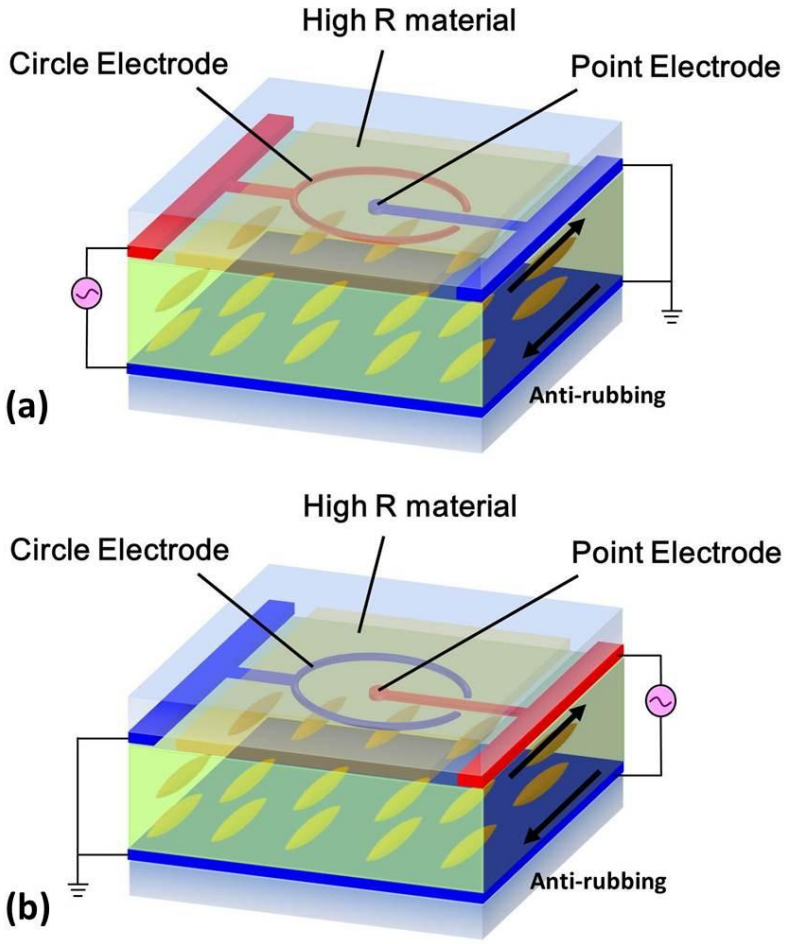

Fig. 5-9 sGD-LC lens driven in (a) convex and (b) concave lens mode

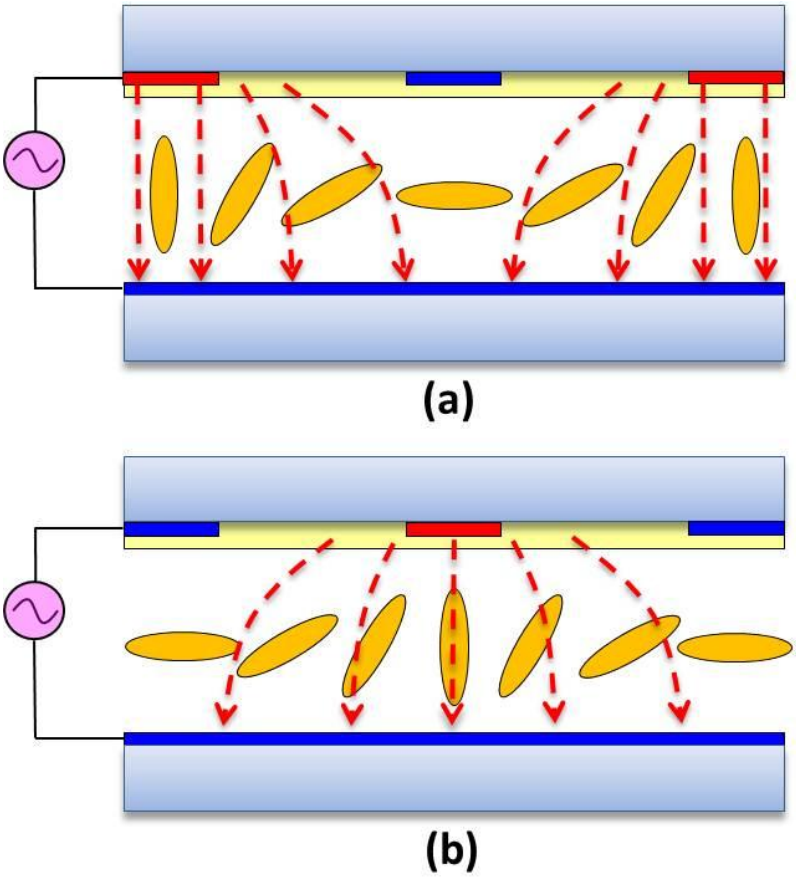

Fig. 5-10 The LC molecules orientation of sGD-LC lenses in (a) convex or (b) concave mode. The electric fields from the controlled electrodes are expressed by the red dotted lines.

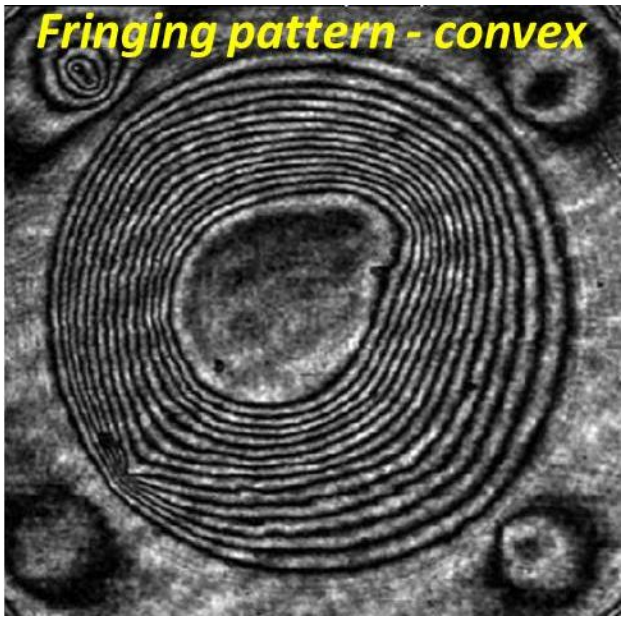

(a)

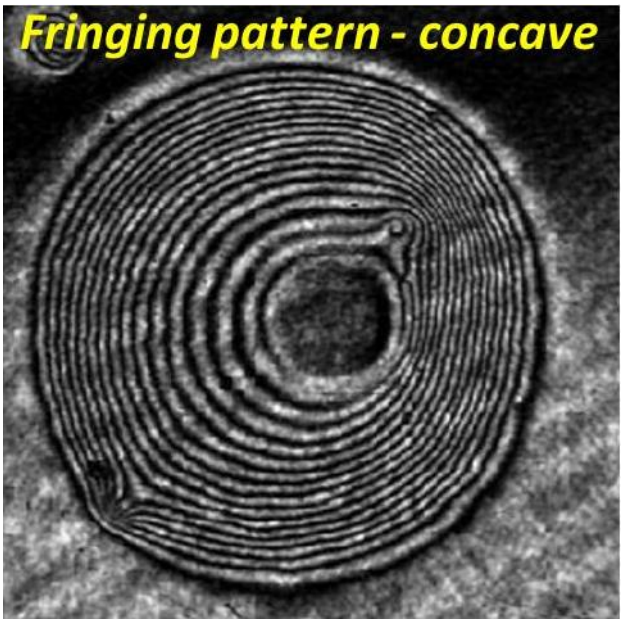

(b)

Fig. 5-11 Fringing patterns of sGD-LC lens in (a) convex lens mode and (b) in concave lens mode. It is difficult to identify the optical properties of two different modes with the fringing patterns.

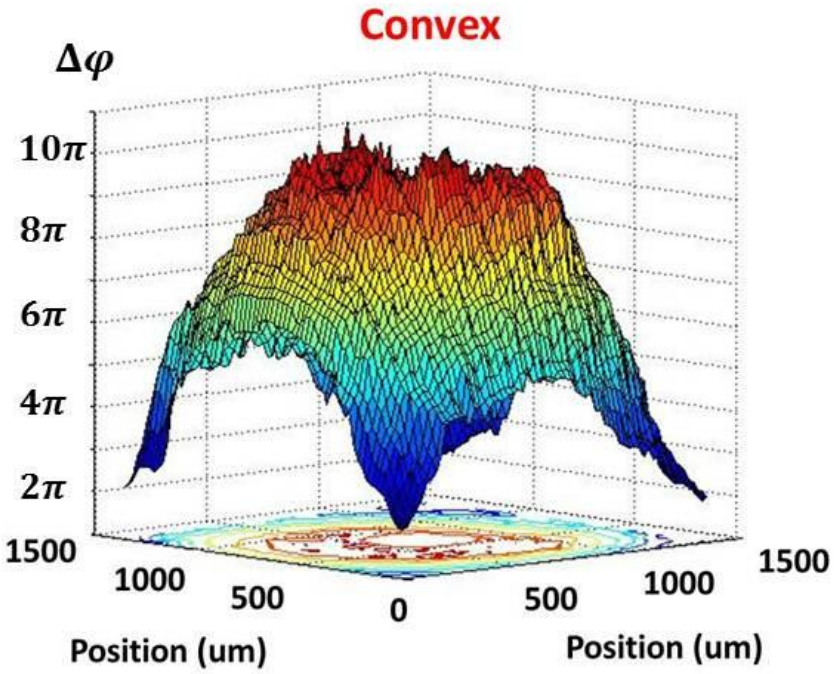

(a)

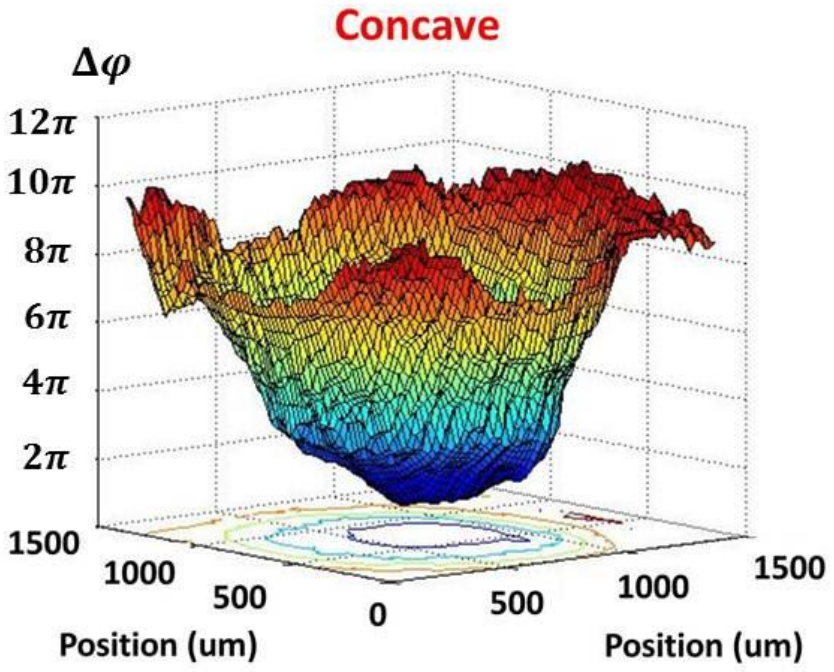

(b)

Fig. 5-12 The phase retardation distribution of sGD-LC lens in (a) convex lens mode and (b) concave lens mode calculated by FCPM method, which illustrate the optical path variation on the border and the center.

5.5 Summary

As shown in Fig. 4-8 and Fig. 4-9, the 3D profile of LC lens can be reconstructed by the include angles between the laser polarization and the LC directors, which were measured with the fluorescent light intensity emitted from the fluorescence dyes. With the birefringence formula in **Eq. 2- 8**, we can calculate the refractive index distribution of LC lens. The optical properties of LC lenses can be considered as GRIN lenses.

The first order optics was verified by comparing the phase retardation variation of LC lenses from the ideal lens formula, the fringing patterns, and the FCPM method. In our experiments, the convex and concave LC lenses were also compared since the FCPM method can show the exact phase retardation which more clearly identify the optical properties of the LC lenses.

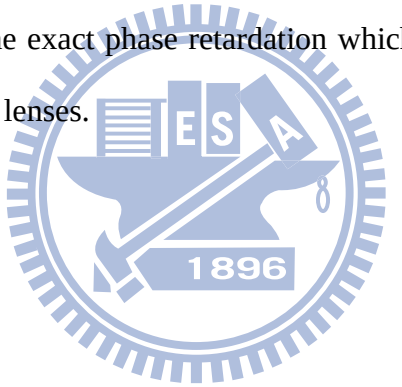

Chapter 6

Conclusion and Future Works

6.1 Conclusion

Compare to the conventional fixed focus lenses made up of glass or polymer, the liquid crystal lenses (LC lenses) have the advantage that focal lengths are electric tunable. The zoom lens systems are usually achieved by adjusting the distances between the multi-lenses groups, which occupy a large volume for the mechanical movement. However, it can much reduce the volume and weight of imaging systems by replacing the glass lenses with slighter and thinner tunable-focus LC lenses.

The lens effects of LC lenses are achieved by the optical path difference (OPD) induced while light propagating through LC lenses. To investigate the optical properties of LC lenses, the profile of the LC molecules is usually observed to determine the optical path length (OPL) of the LC lens. Conventionally, the fringing pattern, which captures the white-black stripes of the linear polarized light phase variation, is used for the observation of the relative phase retardation of LC lenses.

However, the fringing patterns show the integral results of the relative phase retardation, but loss the detail information such as the refractive index of LC molecules and the LC director variation. In this thesis, the Fluorescence Confocal Polarizing Microscopy was proposed to observe the molecular orientation inside the LC lenses. With the fluorescence dyes in 0.01% of weight was doping into LC cells, the LC directors can be measured by the fluorescent light intensity emitted from the fluorescence dye molecules whose dipoles will be along to the LC molecules, as shown in Eq. 4-1 .

Since the LC orientation was known, we enabled the construction of 3D profile

for index distribution with the birefringence formula in Eq. 2- 8. The optical properties of LC lenses can be easily calculated with the effective index distribution of LC molecules. In this thesis, we proposed two spherical LC lens structures and demonstrated the method for investigating LC lens optical properties by the FCPM. The first order optics has been verified by the phase retardation variation as shown in Fig. 5-8. The convex and concave LC lens modes which were difficult to identify by conventional fringing patterns, also have been clearly illustrated with the exact phase retardation of LC lenses by FCPM. For advanced design, FCPM method is necessary for the analysis of LC lenses.

6.2 Future works

LC lenses have advantages that can much save the volume and weight of the conventional imaging systems with the electrical tunable focal lengths. The optical designs of LC lenses become more and more important in the future. The FCPM method can be utilized to observe the refractive index distribution of the LC lens, which the refractive index is necessary in the optical simulation tools since the LC lenses are usually considered as one kind of GRIN lenses.

Although the lens power and performance are not high enough at present, we can adjust a conventional zoom lens behind the LC lens to solve the aberration of the LC lenses, as shown in Fig. 6-1. The refractive index variation of LC lenses measured by FCPM method can help the optical designs of the conventional lens groups. Furthermore, the optical designs of the LC lens-only system can be achieved by the simulation tools. Even the rotation and movement of LC molecules can also be observed by FCPM method, only if the laser scanning speed is improved under the order of 10^{-3}sec.

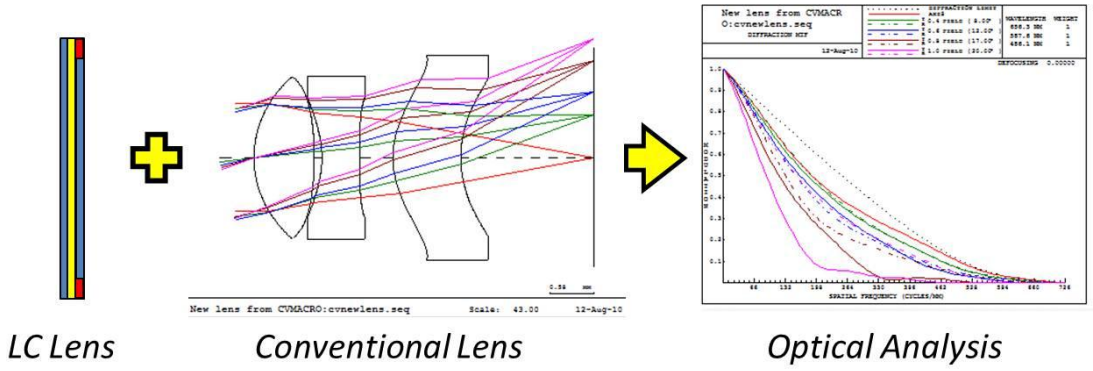

Fig. 6-1 The simulation process that the aberration of LC lens can be solved by the conventional lens group.

Actually, the FCPM method can observe not only the stable state of LC lens, but also the rotation process of LC molecules driven with electric field. The temporal analysis of LC directors in the LC lens was possible with the 3D profile constructed by the FCPM method. For example, the phenomenon that LC lens will focus twice while applied with overload voltage cannot be easily illustrated with fringing patterns or simulation results. However, the LC directors variation measured by the FCPM method shows that phenomenon is a transition state which caused with the rotating speed difference of the LC molecules on the center or the border. With the temporal variation of the fluorescence intensity from LC layers, as shown in Fig. 6-2,we can more detail observe the movement of LC molecules driven with different electric fields, which much helps the LC lens designs.

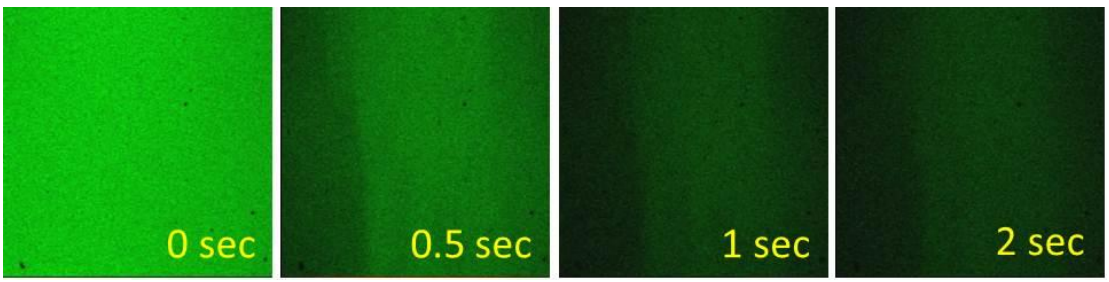

Fig. 6-2 Temporal variation of the fluorescence intensity emitted from the cylindrical LC lens driven with 65Volt (Vrms).

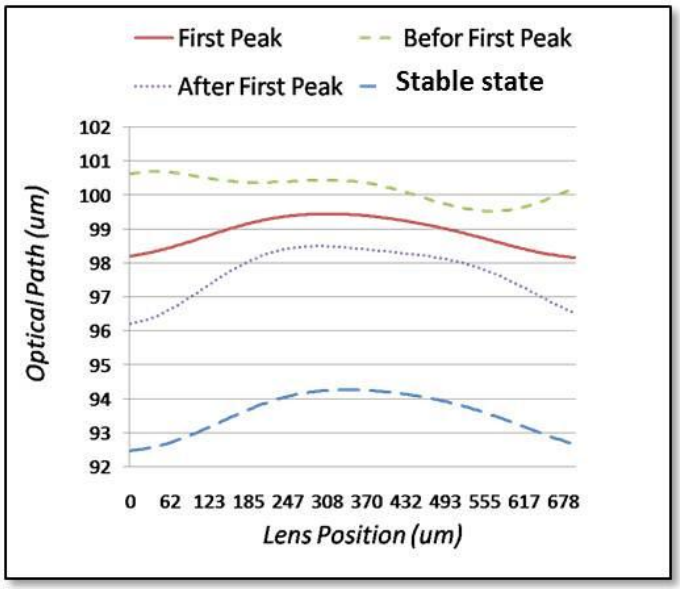

Fig. 6-3 The optical path length variation of the cylindrical LC lens driven with 65V at different time. The variation curve at the first focusing peak and the stable state were similar.

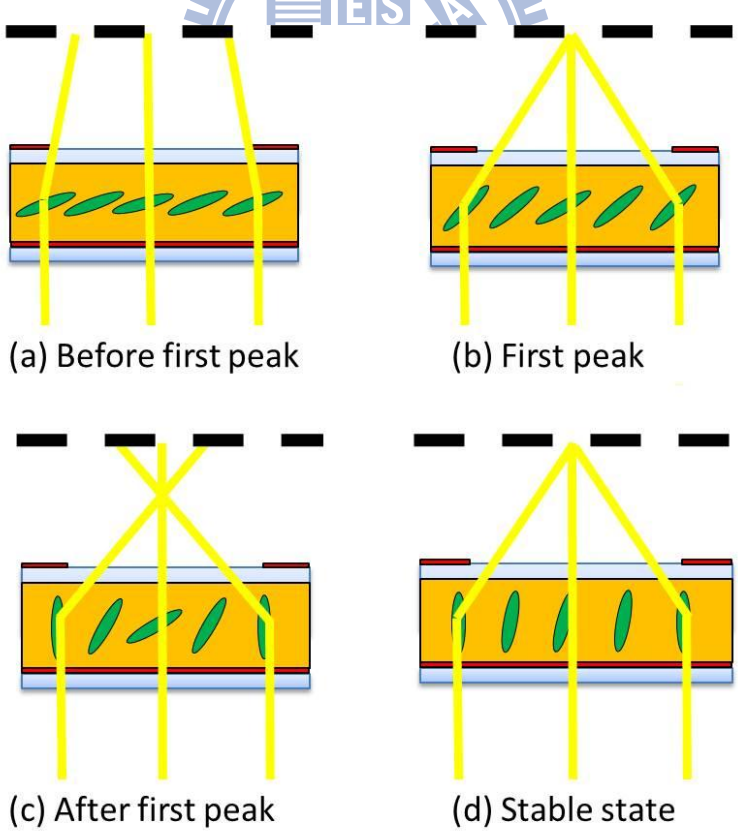

Fig. 6-4 The schematic of LC molecules orientation in the cylindrical LC lens driven with 65V, at different time during the focusing process.

Reference

[1] H. Ren, et al., "Electronically controlled liquid crystal yields tunable-focallength lenses," SPIE's oemagazine, vol. 4, pp. 25-27, 2004.

[2] http://zh.wikipedia.org/wiki/File:Focus_in_an_eye.svg.

[3] S. Kuiper, et al., "Variable-focus liquid lens for miniature cameras," Applied Physics Letters, vol. 85, pp. 1128-1130, 2004.

[4] B. Hendriks, et al., "Electrowetting-based variable-focus lens for miniature systems," Optical review, vol. 12, pp. 255-259, 2005.

[5] H. Oku, et al., "High-speed liquid lens with 2 ms response and 80.3 nm root-mean-square wavefront error," Applied Physics Letters, vol. 94, pp. 221108-221110, 2009.

[6] J. Y. An, et al., "Eye-shaped coplanar variable liquid lens using spherical polymer encapsulation," in Proceedings of IEEE International Conference on Optical MEMS and Nanophotonics (OPT MEMS), Sapporo, pp. 17-18, 9-12 Aug. 2010.

[7] H. Yang, et al., "Low voltage piezoelectricity actuating variable focus plano-convex liquid lens module fabrication," in Proceedings of IEEE Symposium on Design Test Integration and Packaging of MEMS/MOEMS (DTIP), Seville, pp. 119-123, 5-7 May 2010.

[8] T. Kamei, et al., "Contact-lens type of micromachined hydrogenated amorphous Si fluorescence detector coupled with microfluidic electrophoresis devices," Applied Physics Letters, vol. 89, pp. 114101-114101-3, 2006.

[9] S. K. Y. Tang, et al., "Dynamically reconfigurable liquid-core liquid-cladding lens in a microfluidic channel," Lab on a Chip, vol. 8, pp. 395-401, 2008.

[10] B. Berge, et al., "Variable focal lens controlled by an external voltage: an

application of electrowetting," The European Physical Journal E: Soft Matter and Biological Physics, vol. 3, pp. 159-163, 2000.

[11] H. Ren, et al., "Variable-focus liquid lens by changing aperture," Applied Physics Letters, vol. 86, pp. 211107-211109, 2005.

[12] H. Ren, et al., "Tunable-focus liquid lens controlled using a servo motor," Optics Express, vol. 14, p. 8031-8036, 2006.

[13] C. C. Cheng, et al., "Dielectrically actuated liquid lens," Optics Express, vol. 15, pp. 7140-7145, 2007.

[14] H. Ren, et al., "Variable-focus liquid lens," Optics Express, vol. 15, pp. 5931-5936, 2007.

[15] K. Kondo, et al., "Liquid crystal display device," U. S. Patent 5598285, Jan. 28, 1997.

[16] H. Sato, et al., "Liquid crystal display device," U. S. Patent 5712652, Jan. 27, 1998.

[17] M. Ares, et al., "Active optics null test system based on a liquid crystal programmable spatial light modulator," Applied optics, vol. 49, pp. 6201-6206, 2010.

[18] B. R. Boruah, "Zonal wavefront sensing using a liquid crystal spatial light modulator," in Proceeding of SPIE International Conference on Practical Holography XXIV: Materials and Applications, San Francisco, California, USA., vol. 7619, p. 76190G, 24 Jan., 2010.

[19] S. Sato, "Liquid-crystal lens-cells with variable focal length," Japanese Journal of Applied Physics, vol. 18, pp. 1679-1684, 1979.

[20] H. Ren, et al., "Tunable-focus flat liquid crystal spherical lens," Applied Physics Letters, vol. 84, pp. 4789-4791, 2004.

[21] H. Ren, et al., "Adaptive liquid crystal lens with large focal length tunability,"

Optics Express, vol. 14, p. 11292-11298, 2006.

[22] H. Ren, et al., "Liquid crystal lens with large focal length tunability and low operating voltage," Optics Express, vol. 15, p. 11328-11335, 2007.

[23] B. Wang, et al., "Lens of electrically controllable focal length made by a glass lens and liquid-crystal layers," Applied optics, vol. 43, pp. 3420-3425, 2004.

[24] E. A. Salen, et al., "Fundamentals of Optics." Hoboken, N.J.: Wiley-Interscience, 2007.

[25] http://en.wikipedia.org/wiki/Liquid_crystal.

[26] M. Newhouse, et al., "Effect of Axial Perturbation of GRIN Lens Performance," Applied optics, vol. 21, pp. 990-992, 1982.

[27] L. Yi-Hsin, et al., "Tunable-focus cylindrical liquid crystal lenses," Japanese Journal of Applied Physics, vol. 44, pp. 243-244, 2005.

[28] A. Naumov, et al., "Liquid-crystal adaptive lenses with modal control," Optics Letters, vol. 23, pp. 992-994, 1998.

[29] Y.-M. Lin, "Gradient Driven Liquid Crystal Lens Exhibiting Ultra-Fast Focusing by Low Operating Voltage," Master, Institute of Electro-Optical Engineering, National Chiao Tung University, Hsinchu, Taiwan, ROC, 2010.

[30] Y. P. Huang, et al., "2D/3D switchable autostereoscopic display with multi electrically driven liquid crystal (MeD LC) lenses," Journal of the Society for Information Display, vol. 18, p. 642, 2010.

[31] T. Wilson, "Confocal microscopy." London, UK: Academic Press, 1990.

[32] T. R. Corle, et al., "Confocal scanning optical microscopy and related imaging systems." San Diego, CA: Academic Press, 1996.

[33] R. H. Webb, "Confocal optical microscopy," Reports on Progress in Physics, vol. 59, pp. 427-471, 1996.

[34] C. J. R. Sheppard, et al., "Confocal laser scanning microscopy. "Oxford: BIOS

Scientific Publishers, 1997.

[35] W. White, et al., "Real space measurement of structure in phase separating binary fluid mixtures," Physical review letters, vol. 75, pp. 3012-3015, 1995.

[36] J. Nephew, et al., "Reaction-induced phase separation dynamics: a polymer in a liquid crystal solvent," Physical review letters, vol. 80, pp. 3276-3279, 1998.

[37] J. Korlach, et al., "Characterization of lipid bilayer phases by confocal microscopy and fluorescence correlation spectroscopy," Proceedings of the National Academy of Sciences of the United States of America, vol. 96, p. 8461-8466, 1999.

[38] I. Dierking, "Fluorescence confocal polarizing microscopy: Imaging liquid crystal director fields in three dimensions," ChemPhysChem, vol. 2, pp. 663-664, 2001.

[39] I. Smalyukh, et al., "Three-dimensional imaging of orientational order by fluorescence confocal polarizing microscopy," Chemical physics letters, vol. 336, pp. 88-96, 2001.

[40] O. Lavrentovich, "Fluorescence confocal polarizing microscopy: Three-dimensional imaging of the director," Pramana, vol. 61, pp. 373-384, 2003.

[41] L. M. Blinov , et al., "Electrooptic effects in liquid crystal materials." New York: Springer, 1993.

[42] Y.C. Chen. "Extremely-fast FocusingGradient Driven Liquid Crystal Lens Driven by Ultra-low Operating Voltage," International Display Manufacturing Conference, Taipei, ROC, Apr. 18-21, 2011.